JOURNAL OF GUIDANCE, CONTROL, AND DYNAMICS
Vol. 34, No. 1, January–February 2011

Multivehicle Coordination in an Estimated Time-Varying Flowfield

Cameron Peterson* and Derek A. Paley†
University of Maryland, College Park, Maryland 20742

DOI: 10.2514/1.50036

Unmanned vehicles are an effective platform for tracking, surveillance, and reconnaissance missions. Existing control algorithms promote collaboration of unmanned aerial vehicles and other autonomous vehicles. However, these algorithms often fail to account for the degradation of control performance caused by flowfields. This paper presents decentralized multivehicle coordination algorithms designed for operation in a spatially or temporally varying flowfield. Each vehicle is represented using a Newtonian particle traveling at constant speed relative to the flow and subject to a steering control. An algorithm is described that stabilizes a circular formation in a time-varying spatially nonuniform flowfield, assuming that the flowfield is known and does not exceed the particle speed relative to the flow. For a time-varying and spatially uniform flowfield, an algorithm is provided to stabilize a circular formation in which the temporal spacing between particles is regulated. These algorithms are extended by relaxing the assumption that the flow is known: each particle dynamically estimates the flow and uses that estimate in the control. It is shown that including a turning-rate bound does not alter the main results. The theoretical results are supported by numerical simulations that illustrate the coordinated encirclement of a maneuvering target.

Nomenclature

c_k	=	center of circle traversed by particle k
$f_k(t)$	=	flow velocity at position r_k and time t
$\hat{f}_k(t)$	=	estimated flow velocity at position r_k and time t
i	=	imaginary unit
K	=	control gain
l	=	maximum velocity of a moving target
N	=	number of particles
P	=	$N \times N$ projector matrix
P_k	=	kth row of matrix P
r_k	=	position of particle k
$\hat{r}_k$	=	estimated position of particle k
$\dot{r}_k$	=	inertial velocity of particle k
$s_k(t)$	=	inertial speed of particle k at time t
T	=	period of revolution around a circular orbit
u_k	=	angular rate of change of the velocity orientation relative to the flow of particle k
$u_{\max}$	=	maximum turn rate
γ_k	=	orientation of the inertial velocity of particle k
θ_k	=	orientation of the velocity of particle k relative to the flow
ν_k	=	angular rate of change of the inertial-velocity orientation for particle k
ρ	=	turning radius of a moving target
ψ_k	=	time phase of particle k
ω_0	=	constant angular rate

Subscript

j, k	=	particle and phase indices, $1, \ldots, N$

I. Introduction

AUTONOMOUS vehicles in the air and ocean provide a cost-effective robust approach for tracking, surveillance, and reconnaissance missions. A cooperating team of vehicles can coordinate data collection and provide persistent coverage of continuous spatiotemporal processes, like environmental fields, or discrete processes, like moving ground targets. Unmanned platforms are particularly well suited for multi-agent coordinated missions that require synoptic area coverage with consistent revisit rates. Many algorithms are capable of providing decentralized control of multiple agents with mobility and communication constraints [1–10]. These algorithms have been adapted for use in a wide variety of applications, including aerobiological sampling [11], gathering in situ measurements of severe storms [1], path planning of autonomous underwater gliders [12], and environmental boundary tracking [13]. A particular application highlighted in this paper is the coordinated encirclement of a maneuvering target [2–4,14].

One obstacle limiting the performance of existing control algorithms is the presence of an external flowfield that may represent a significant fraction of a vehicle's velocity. Some existing algorithms support operations in spatially uniform flowfields [15,16]. However, the authors are not aware of any existing theoretically justified motion-coordination algorithms for spatially and temporally varying flowfields. This problem is partially addressed here by providing decentralized control algorithms for motion coordination in a moderate time-varying flowfield (i.e., between 10 and 99% of the platform speed). This work extends previous work in which decentralized control algorithms are presented for a time-invariant flowfield [17,18]. Strong flowfields are not addressed here (i.e., having speed greater than the platform speed relative to the flow); this subject is being studied as part of ongoing research.

This paper builds upon prior research on cooperative control for autonomous vehicles. Frew et al. showed two vehicles collaborating to encircle a target while maintaining a constant angular separation [2]. The separation was preserved with a variable-speed controller while the distance to the target was regulated by following Lyapunov-based guidance vector fields. The vector fields steered the vehicles in a loiter circle at a desired standoff radius. This approach was expanded by Summers et al., who relaxed the assumption that the flowfield or target velocity was known and allowed cooperative control of two or more vehicles [3]. However, a variable-speed control design has the potential disadvantage of being fuel inefficient [3].

Constant-speed controllers were provided by Sepulchre et al. for a flow-free environment, maintaining a uniform separation of vehicles traveling around a circle using decentralized steering control [6]. In the absence of a flowfield, the vehicles can be equally spaced in both space and time. Maintaining an equal angular separation in the presence of a flowfield may not be possible with a unit-speed vehicle model. Klein and Morgansen proposed a temporal-spacing control

Received 24 March 2010; revision received 24 June 2010; accepted for publication 26 September 2010.

*Graduate Student, Department of Aerospace Engineering; cammykai@yahoo.com. Student Member AIAA.

†Assistant Professor, Department of Aerospace Engineering; dpaley@umd.edu. Associate Fellow AIAA.

for tracking a constant-velocity target [14]; the algorithm placed a restriction on the number of vehicles in the formation. Kingston proposed a sliding-mode algorithm that would allow for an unlimited number of cooperating vehicles to encircle moving targets in a steady, uniform external flowfield [9]. Paley and Peterson provided a Lyapunov-based control design to encircle a centroid in a time-invariant flowfield [18]. Paley et al. [19] and Techy et al. [20] also showed that stabilization of a circular formation in a flowfield can be extended to stabilization of a convex loop.

Another approach used to develop decentralized cooperative control algorithms is to choose vehicle trajectories that optimize the potential information gain of the system. The total information of the system is equal to the linear combination of the information of the individual vehicles. Grocholsky et al. used the information filter along with decentralized fusion algorithms as a means to guide vehicles to map out the terrain of an area [21]. Using the Fisher information matrix, Ousingsawat and Campbell combined individual vehicle information in a cost function to determine optimal vehicle paths for reconnaissance of stationary targets [22]. They used target clustering and cost bounding to make the algorithm computationally tractable. Zhou and Roumeliotis extended this approach to track a moving target with a team of mobile sensors [23]. The sensors provide range-only measurements and assume constraints on the vehicle speed. Under these restrictions, they found the optimal trajectory that minimized position uncertainty for the target.

As in prior work [18], each autonomous vehicle is modeled as a Newtonian particle that travels at unit speed relative to the flow. The flowfield may be spatially or temporally varying, but its magnitude is assumed to be less than the speed of the particle. This ensures that each particle will always maintain forward progress over ground. The particle is subject to a steering control that is justified using Lyapunov-based analysis, the invariance principle, and an invariancelike principle for nonautonomous systems. (The latter is invoked in the analysis of the closed-loop particle model with a time-varying flowfield.)

The steering control is designed to drive the particles into a circular formation centered on either an arbitrary location or a specific target. By accounting for target acceleration, one can follow targets as they execute realistic maneuvers. Additionally, target encirclement is presented for a time-splay configuration in a time-varying uniform flowfield. A time-splay configuration regulates the temporal spacing between particles. Regulating the temporal separation between particles is a first step toward collision avoidance. However, it does not guarantee separation of the particles while they transition to the configuration. Overall collision avoidance is not addressed in this paper and is left as a future topic of study.

The contribution of this paper is the synthesis of theoretically justified control algorithms to cooperatively stabilize vehicles to the following formations: 1) a circular formation in a known spatially and temporally varying flowfield, 2) a time-splay configuration in a known time-varying spatially uniform flowfield, and 3) both circular and time-splay configurations in an estimated flowfield. The known-flow controller is augmented with a dynamic controller that estimates the flowfield and uses this estimate in the control law. It is also shown that these controllers operate under a restricted turn rate. Accelerating frame dynamics are provided so that the control algorithms may be applied to encircling maneuvering targets. Simulation results demonstrate the utility of these control algorithms.

The paper proceeds as follows. Section II examines the Newtonian-particle model used to describe the motion of a fleet of autonomous vehicles in an external flowfield. Section III develops Lyapunov-based circular control algorithms for the particle model in an external flowfield. Section IV discusses control laws for use in an external flow when aspects of the flowfield are unknown. Section V provides algorithms to stabilize circular formations in a spatially uniform or rotating flowfield with a turn-rate constraint. Section VI derives the equations of motion for an accelerating frame and provides performance results for circular configurations in a variety of flowfields induced in a moving reference frame attached to a maneuvering target. Section VII summarizes the results and highlights some ongoing work.

II. Dynamic Model of a Vehicle in a Time-Varying Flowfield

Each unmanned vehicle is modeled as a planar self-propelled particle moving at unit speed relative to a spatially and temporally variable flowfield. This model has been adopted frequently in previous works for a flow-free environment [5,6]. Each particle is steered by a control force that is perpendicular to the velocity relative to the flow. The steering control, denoted by u, is constrained for many autonomous vehicles. For example, with an unmanned aerial vehicle (UAV), one factor restricting the steering control is the bank angle of the aircraft. Since there is a finite limit to the degree to which a UAV can bank, the steering control is bounded. To model this effect, a bound is placed on the turn rate by saturating u.

The positions of N individual particles are denoted as r_k, where $k \in \{1, \ldots, N\}$. The inertial velocity of the kth particle is denoted by $\dot{r}_k$. The particles do not accelerate tangentially to their path and thus move with unit velocity $e^{i\theta_k}$ relative to the flowfield. The flowfield at r_k and time t is denoted by $f_k(t) = f(r_k, t)$. The equations of motion for particle k are

$$\dot{r}_k = e^{i\theta_k} + f_k(t); \qquad \dot{\theta}_k = \mathrm{sat}(u_k; u_{\max}) \tag{1}$$

where $u_{\max} > 0$, and

$$\mathrm{sat}\,(u_i; u_{\max}) = \begin{cases} -u_{\max} & u_k < -u_{\max} \\ u_k & -u_{\max} \le u_k \le u_{\max} \\ u_{\max} & u_k > u_{\max} \end{cases} \tag{2}$$

For a vehicle with an unbounded turning rate, $u_{\max} = \infty$, and the model in Eq. (1) becomes

$$\dot{r}_k = e^{i\theta_k} + f_k(t); \qquad \dot{\theta}_k = u_k \tag{3}$$

Let $\gamma_k = \arg(\dot{r}_k)$ equal the orientation of the inertial velocity of the kth particle and $s_k(t) = s(t, r_k, \theta_k) = |\dot{r}_k|$ denote its magnitude. The particle model without the turn-rate constraint is equivalent to [18]

$$\dot{r}_k = s_k(t)e^{i\gamma_k}; \qquad \dot{\gamma}_k = \nu_k \tag{4}$$

where ν_k is the angular rate of change of the inertial-velocity orientation. Note that it is required that $|f_k(t)| < 1$ for all k and t to ensure $s_k(t) > 0$. This assumption guarantees that the particles will always exhibit forward motion in an inertial reference frame.

Figure 1 illustrates the Newtonian-particle model for an air vehicle. Figure 1a shows the dynamics in a flowfield; the inertial velocity is the sum of the velocity relative to the flow plus the velocity of the flow relative to the inertial (ground fixed) frame. Figure 1b shows the kth particle in the complex plane. The particle is located at r_k, and its velocity relative to the flow is $e^{i\theta_k}$. In the presence of a flowfield f_k, the inertial velocity of the particle is $\dot{r}_k = e^{i\theta_k} + f_k = s_k(t)e^{i\gamma_k}$. The steering control is applied in the direction $ie^{i\theta_k}$, which is perpendicular to the velocity relative to the flow.

Section III discusses stabilization of circular formations using the unconstrained model in Eq. (4) in a known flow. Section IV continues to use the unconstrained model but relaxes the known-flow assumption. Section V invokes the turn-rate constraint model in Eq. (1).

The controller design focuses on obtaining a suitable ν_k; u_k is seen as the low-level controller used as input for an autonomous vehicle and should be recoverable from ν_k. Figure 1 exhibits the following relationship [18] between θ_k and γ_k[‡]:

$$\sin\theta_k = s_k(t)\sin\gamma_k - \langle f_k(t), i\rangle \tag{5}$$

$$\cos\theta_k = s_k(t)\cos\gamma_k - \langle f_k(t), 1\rangle \tag{6}$$

which gives

[‡]The inner product $\langle x, y\rangle = Re\{\bar{x}y\}$ is used, where $x, y \in \mathbb{C}$ and $\bar{x}$ is the complex conjugate of x.

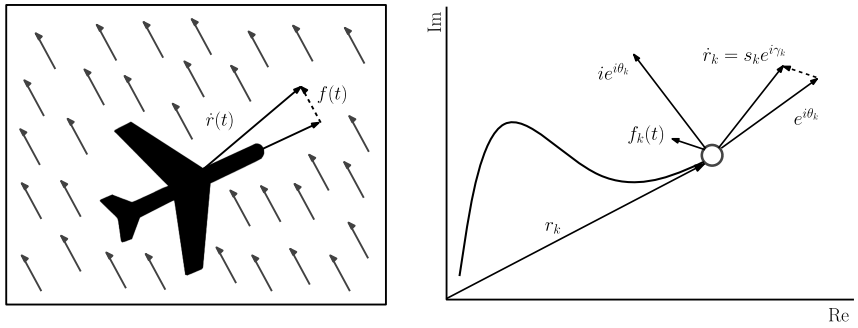

a) **b)**

Fig. 1 The inertial velocity of a particle is the sum of the flow velocity relative to the ground and the velocity of the particle relative to the flow.

$$\tan\gamma_k = \frac{\sin\theta_k + \langle f_k(t), i\rangle}{\cos\theta_k + \langle f_k(t), 1\rangle} \tag{7}$$

Differentiating Eq. (7) with respect to time and substituting in Eqs. (5) and (6) yields

$$\begin{aligned}\dot{\gamma}_k &= (\cos\theta_k\cos\gamma_k + \sin\theta_k\sin\gamma_k)s_k^{-1}(t)\dot{\theta}_k \\ &\quad + \langle \dot{f}_k(t), i\rangle s_k^{-1}(t)\cos\gamma_k - \langle \dot{f}_k(t), 1\rangle s_k^{-1}(t)\sin\gamma_k \\ &= [1 - s_k^{-1}(t)\langle e^{i\gamma_k}, f_k(t)\rangle]u_k + s_k^{-1}(t)\langle ie^{i\gamma_k}, \dot{f}_k(t)\rangle \triangleq \nu_k\end{aligned} \tag{8}$$

with

$$\dot{f}_k(t) = \frac{\partial f_k}{\partial r_k}\dot{r}_k + \frac{\partial f_k}{\partial t} \tag{9}$$

Solving for $u_k(t)$ provides the steering control as a function of ν_k:

$$u_k(t) = \frac{s_k(t)\nu_k - \langle ie^{i\gamma_k}, \dot{f}_k(t)\rangle}{s_k(t) - \langle e^{i\gamma_k}, f_k(t)\rangle} \tag{10}$$

The preceding equation is well defined everywhere, because the denominator satisfies [18]

$$s_k(t) - \langle e^{i\gamma_k}, f_k(t)\rangle \geq s_k(t) - |f_k(t)| > 0$$

In the following examples, $s_k(t)$ and $u_k(t)$ are calculated for a time-varying spatially uniform flowfield and a time-varying spatially nonuniform flowfield.

For a time-varying spatially uniform flowfield, let a uniform flow be defined as $f(t) = \eta(t)e^{i\phi(t)}$, where $\eta(t)$ is the magnitude of the flow and $\phi(t)$ is the direction. The k subscript is dropped from $f(t)$ since a uniform flow at time t is identical for all particles. It is assumed that $|\eta(t)| < 1$ for all t to ensure that $s_k(t) > 0$. The inertial speed is

$$\begin{aligned}s_k(t) &= \sqrt{Re\{[\eta(t)e^{i\phi(t)} + e^{i\theta_k}][\eta(t)e^{-i\phi(t)} + e^{-i\theta_k}]\}} \\ &= \sqrt{1 + [\eta(t)]^2 + 2\eta(t)[\cos\theta_k\cos\phi(t) + \sin\theta_k\sin\phi(t)]}\end{aligned} \tag{11}$$

where $s_k(t)$ is expressed as a function of γ_k and $f(t)$ by substituting Eqs. (5) and (6) into Eq. (11) and rearranging the result to obtain the quadratic equation

$$\begin{aligned}&[s_k(t)]^2 - 2\eta(t)[\cos\gamma_k\cos\phi(t) + \sin\gamma_k\sin\phi(t)]s_k(t) \\ &\quad + [\eta(t)]^2 - 1 = 0\end{aligned} \tag{12}$$

Equation (12) has the following solution (using the positive root, since $s_k(t) > 0$):

$$\begin{aligned}s_k(t) &= \eta(t)[\cos\gamma_k\cos\phi(t) + \sin\gamma_k\sin\phi(t)] \\ &\quad + \sqrt{1 + [\eta(t)]^2[(\cos\gamma_k\cos\phi(t) + \sin\gamma_k\sin\phi(t))^2 - 1]} \\ &= \langle e^{i\gamma_k}, f(t)\rangle + \sqrt{1 - \langle ie^{i\gamma_k}, f(t)\rangle^2}\end{aligned} \tag{13}$$

By substituting $f(t) = \eta(t)e^{i\phi(t)}$ and $\dot{f}(t) = \dot{\eta}(t)e^{i\phi(t)} + i\eta(t)\dot{\phi}(t)e^{i\phi(t)}$ into Eq. (10), $u_k(t)$ is found to be

$$u_k(t) = \frac{\nu_k s_k(t) + \dot{\eta}(t)\sin[\gamma_k - \phi(t)] - \eta(t)\dot{\phi}(t)\cos[\gamma_k - \phi(t)]}{s_k(t) - \eta(t)\cos[\gamma_k - \phi(t)]} \tag{14}$$

This calculation shows that, in order to use ν_k to compute the turn-rate control u_k in a time-varying flowfield, the following variables need to be known: 1) the magnitude of the flowfield $\eta(t)$, 2) the rate of change of the flowfield $\dot{\eta}(t)$, and 3) the difference between the direction of the flow and the orientation of the inertial velocity, $\gamma_k - \phi(t)$.

For the example of a time-varying spatially nonuniform flowfield, let $f_k(t) = \beta_k(t) + i\alpha_k(t)$, where $\beta_k(t) = \beta(t, r_k)$ and $\alpha_k(t) = \alpha(t, r_k)$ are the real and imaginary components of the flowfield at r_k. Computing $s_k(t)$ yields

$$\begin{aligned}s_k(t) &= \sqrt{Re\{[e^{i\theta_k} + \beta_k(t) + i\alpha_k(t)][e^{-i\theta_k} + \beta_k(t) - i\alpha_k(t)]\}} \\ &= \sqrt{1 - [\beta_k(t)]^2 - [\alpha_k(t)]^2 + 2s_k(t)(\alpha_k(t)\sin\gamma_k + \beta_k(t)\cos\gamma_k)}\end{aligned} \tag{15}$$

Next, $s_k(t)$ is expressed as a function of γ_k and $f_k(t)$. Squaring both sides of Eq. (15) and solving the resulting quadratic equation (using the positive root since $s_k(t) > 0$) gives

$$\begin{aligned}s_k(t) &= \alpha_k(t)\sin\gamma_k + \beta_k(t)\cos\gamma_k \\ &\quad + \sqrt{1 - [\alpha_k(t)\cos\gamma_k - \beta_k(t)\sin\gamma_k]^2} = \langle e^{i\gamma_k}, f_k(t)\rangle \\ &\quad + \sqrt{1 - \langle ie^{i\gamma_k}, f_k(t)\rangle^2}\end{aligned} \tag{16}$$

To solve for $u_k(t)$, let the position of particle k be $r_k = x_k + iy_k$. The time derivative of $f_k(t)$ is

$$\dot{f}_k(t) = \frac{\partial\beta_k}{\partial x_k}\dot{x}_k + \frac{\partial\beta_k}{\partial y_k}\dot{y}_k + \frac{\partial\beta_k}{\partial t} + i\left(\frac{\partial\alpha_k}{\partial x_k}\dot{x}_k + \frac{\partial\alpha_k}{\partial y_k}\dot{y}_k + \frac{\partial\alpha_k}{\partial t}\right)$$

Substituting $\dot{f}_k(t)$ into Eq. (10) yields

$$u_k(t) = \frac{\nu_k s_k(t) - \sin\gamma_k[(\partial\beta_k/\partial x_k)\dot{x}_k + (\partial\beta_k/\partial y_k)\dot{y}_k + (\partial\beta_k/\partial t)] + \cos\gamma_k[(\partial\alpha_k/\partial x_k)\dot{x}_k + (\partial\alpha_k/\partial y_k)\dot{y}_k + (\partial\alpha_k/\partial t)]}{s_k(t) - \beta_k(t)\cos\gamma_k - \alpha_k(t)\sin\gamma_k} \tag{17}$$

Thus, given the control v_k, the orientation of the inertial velocity γ_k, the flowfield $f_k(t)$, and the directional derivative $\dot{f}_k(t)$, one can solve for u_k, which is the control input to the vehicle model in Eq. (1).

III. Stabilization of a Circular Formation in a Known Flowfield

This section provides decentralized control laws that stabilize a circular formation in a time-varying flowfield. For now, the turning rate constraint is relaxed and it is assumed that the flow is known. Section III.A provides a control law for the model in Eq. (3) to stabilize a circular formation about an arbitrary point in a spatially nonuniform flowfield. In Sec. III.B, a symmetry-breaking virtual particle is introduced that allows the formation center to be specified. The latter algorithm enables the particles to follow a constant-velocity target. (A method is presented to follow a maneuvering target in Sec. VI.) Finally, in Sec. III.C, a circular-formation control law is provided that regulates the temporal spacing of the particles in a spatially uniform flowfield.

A. Circular Formation with an Arbitrary Center

A control law is developed that drives the particles into a circular formation about an arbitrary, fixed point. All of the particles in the circular formation travel in the same direction. In the case of a flow-free environment, setting u_k equal to a constant ω_0 will drive the particles about a fixed center point with radius $|\omega_0|^{-1}$. In the model in Eq. (3), the center of a circular trajectory is [18]:

$$c_k \triangleq r_k + \omega_0^{-1} i \frac{\dot{r}_k}{|\dot{r}_k|} = r_k + \omega_0^{-1} i e^{i\gamma_k} \tag{18}$$

By differentiating Eq. (18) with respect to time, a steering control v_k is derived that drives a single particle around a circle in a time-varying flow. This gives

$$\dot{c}_k(t) = s_k(t) e^{i\gamma_k} - \omega_0^{-1} e^{i\gamma_k} v_k = (s_k(t) - \omega_0^{-1} v_k) e^{i\gamma_k} \tag{19}$$

Equation (19) with $v_k = \omega_0 s_k(t)$ ensures $\dot{c}_k = 0$, which implies the center is fixed. Particle k will traverse a circle with constant radius $|\omega_0|^{-1} = |c_k(0) - r_k(0)|$.

Next, a steering control is proposed that drives all particles to orbit the same center point in the same direction. Let $\mathbf{1} \triangleq (1, \ldots, 1)^T \in \mathbb{R}^N$. In a circular formation, $c_k = c_j$ for all pairs j and k, which implies the condition $P\boldsymbol{c} = 0$ [6], where P is the $N \times N$ projection matrix:

$$P = \operatorname{diag}\{\mathbf{1}\} - \frac{1}{N}\mathbf{1}\mathbf{1}^T \tag{20}$$

This matrix is equivalent to the Laplacian matrix of an all-to-all communication topology [24]. (Since the intent of this paper is to focus on the time-varying aspect of the flowfield, all-to-all communication is assumed even though it is possible to relax this constraint to a topology with limited communication [7].)

Following prior work, choose the Lyapunov function [6]

$$S(\boldsymbol{r}, \boldsymbol{\gamma}) \triangleq \frac{1}{2}\langle \boldsymbol{c}, P\boldsymbol{c} \rangle \tag{21}$$

where $\boldsymbol{r}$, $\boldsymbol{\gamma}$, and $\boldsymbol{c}$ are the vector representations of the particle's inertial positions, orientations, and circular trajectory centers, respectively. Note that S is positive definite in the reduced space of relative centers. It is equal to zero only when $\boldsymbol{c} = c_0\mathbf{1}$ for some $c_0 \in \mathbb{C}$.

The time derivative of S along solutions of Eq. (4) is

$$\dot{S} = \sum_{k=1}^{N} \langle \dot{c}_k, P_k\boldsymbol{c} \rangle = \sum_{k=1}^{N} \langle e^{i\gamma_k}, P_k\boldsymbol{c} \rangle (s_k(t) - \omega_0^{-1} v_k) \tag{22}$$

where P_k is the kth row of the projection matrix P.

The following theorem extends [18] [Theorem 3] to incorporate a time-varying flowfield.

Theorem 1. Let $f_k(t) = f(r_k, t)$, such that $|f_k(t)| < 1 \quad \forall\ k, t$. Choosing the control

$$v_k = \omega_0(s_k(t) + K\langle P_k\boldsymbol{c}, e^{i\gamma_k} \rangle); \qquad K > 0; \qquad \omega_0 \neq 0 \tag{23}$$

forces uniform convergence of solutions of the model in Eq. (4) to the set of circular formations with radius $|\omega_0|^{-1}$ and the direction determined by the sign of ω_0.

Proof. The potential $S(\boldsymbol{r}, \boldsymbol{\gamma})$ is radially unbounded and positive definite in the (complex) codimension one reduced space of relative centers. Under the control in Eq. (23), the time derivative of S along with solutions to Eq. (4) is

$$\dot{S} = -K \sum_{k=1}^{N} \langle P_k\boldsymbol{c}, e^{i\gamma_k} \rangle^2 \leq 0$$

According to an invariancelike theorem for nonautonomous systems ([25], Theorem 8.4), the solutions of Eq. (4) with the control in Eq. (23) converge to the set $\{\dot{S} = 0\}$ in which

$$\langle P_k\boldsymbol{c}, e^{i\gamma_k} \rangle = 0, \quad \forall\ k \tag{24}$$

In this set, the control in Eq. (23) evaluates to $v_k = \omega_0 s_k(t)$ and $\dot{c}_k = 0$, which implies each particle traverses a circle with a fixed center. Therefore, $P_k\boldsymbol{c}$ is constant and must be zero for Eq. (24) to hold. Since the null space of P is spanned by $\mathbf{1}$, then Eq. (24) is satisfied only when $P\boldsymbol{c} = 0$, which implies $c_k = c_j \quad \forall\ k, j$. S decreases over the interval $[t, t + \delta] \quad \forall\ t \geq 0$, for some $\delta > 0$, which implies the set of circular formations with radius $|\omega_0|^{-1}$ is uniformly asymptotically stable ([25], Theorem 8.5). □

Figure 2 illustrates Theorem 1 for a time-varying spatially nonuniform flowfield. It shows the convergence of $N = 5$ particles to a circular formation for which the center was determined by initial conditions. The flowfield is generated by the periodic function

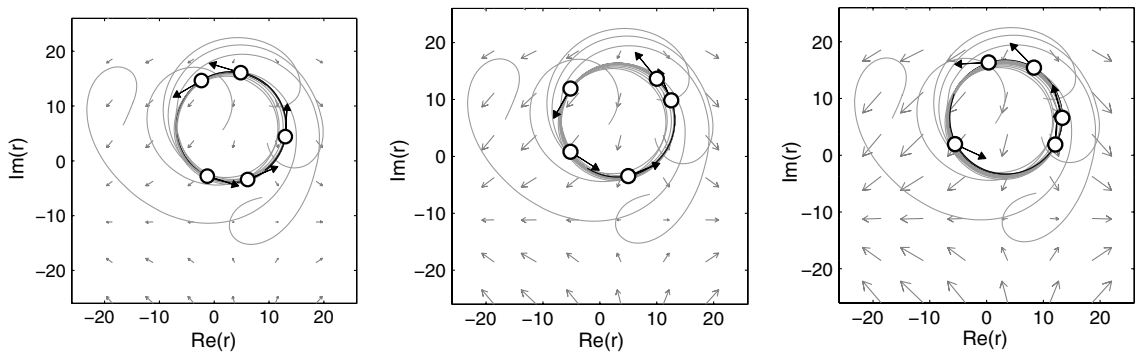

a) t = 200 s **b) t = 400 s** **c) t = 600 s**

Fig. 2 Stabilization of a circular formation with an arbitrary center in a time-varying spatially nonuniform flowfield.

$$f_k(t) = a(t)[\sin(2\pi\omega x_k - \varphi_0) + i\cos(2\pi\omega y_k - \varphi_0)]$$

where $a(t) = 0.75\sin(10t)$, $\omega = 1$, and $\varphi_0 = 10$.

B. Circular Formation with a Prescribed Center

Under the control in Eq. (23), the center of the circular formation depends only on the flowfield and the initial conditions of the particles. By introducing a virtual particle (indexed by $k = 0$) and choosing initial conditions $r_0(0)$ and $\gamma_0(0)$, a center point for the formation is prescribed to be $c_0(0) = r_0(0) + i\omega_0^{-1}e^{i\gamma_0(0)}$. The virtual particle has the dynamics $r_0(t) = s_0(t)e^{i\gamma_0}$ and $\dot{\gamma}_0 = s_0(t)\omega_0$, which implies $c_0(t) = c_0(0)$ by Eq. (19). This makes possible applications such as encirclement of a moving target, where the formation needs to be directed to a specific location that may be moving with piecewise-constant velocity.

Consider the augmented potential $\tilde{S}(\boldsymbol{r}, \boldsymbol{\gamma}) = S(\boldsymbol{r}, \boldsymbol{\gamma}) + S_0(\boldsymbol{r}, \boldsymbol{\gamma})$ [7], where

$$S_0(\boldsymbol{r}, \boldsymbol{\gamma}) = \frac{1}{2}\sum_{k=1}^{N} a_{k0}|c_k - c_0|^2 \tag{25}$$

$a_{k0} = 1$ if particle k is informed of the reference center, and $a_{k0} = 0$ otherwise. The time derivative of Eq. (25) is

$$\dot{\tilde{S}} = \sum_{k=1}^{N}(\langle e^{i\gamma_k}, P_k\boldsymbol{c}\rangle + a_{k0}\langle e^{i\gamma_k}, c_k - c_0\rangle)[s_k(t) - \omega_0^{-1}\nu_k] \tag{26}$$

The following theorem extends ([18] Corollary 3) to incorporate a time-varying flowfield.

Theorem 2. Let $f_k(t) = f(r_k, t)$ satisfy $|f_k(t)| < 1 \quad \forall\ k, t$. Choosing the control

$$\nu_k = \omega_0[s_k(t) + K(\langle e^{i\gamma_k}, P_k\boldsymbol{c}\rangle + a_{k0}\langle e^{i\gamma_k}, c_k - c_0\rangle)]$$
$$K > 0, \qquad \omega_0 \neq 0 \tag{27}$$

where $a_{k0} = 1$ for at least one $k \in 1, \ldots, N$, and zero otherwise, forces uniform convergence of all solutions of the model in Eq. (4) to the set of circular formations centered on c_0 with radius $|\omega_0|^{-1}$ and direction determined by the sign of ω_0.

Proof. The time derivative of the augmented potential $\tilde{S}(\boldsymbol{r}, \boldsymbol{\gamma})$ satisfies

$$\dot{\tilde{S}} = -K\sum_{k=1}^{N}(\langle e^{i\gamma_k}, P_k\boldsymbol{c}\rangle + a_{k0}\langle e^{i\gamma_k}, c_k - c_0\rangle)^2 \leq 0$$

By an invariancelike principle for nonautonomous systems ([25], Theorem 8.4), solutions of Eq. (4) converge to the set $\{\dot{\tilde{S}} = 0\}$ in which

$$\langle e^{i\gamma_k}, P_k\boldsymbol{c}\rangle + a_{k0}\langle e^{i\gamma_k}, c_k - c_0\rangle = 0 \quad \forall\ k \tag{28}$$

If there exists a j such that $a_{j0} = 0$, then Eq. (28) reduces to $\langle e^{i\gamma_j}, P_j\boldsymbol{c}\rangle$ and the control in Eq. (27) becomes $\nu_j = \omega_0 s_j(t)$. Following the proof of Theorem 1, Eq. (28) holds only when $c_k = c_j$ for all pairs k and j. For the informed particles where $a_{k0} = 1$, Eq. (28) becomes

$$\langle e^{i\gamma_k}, c_k - c_0\rangle = 0 \tag{29}$$

This condition is satisfied only if $c_k = c_0$, ensuring that all particles will converge to a circular formation around the prescribed center c_0. The case of $a_{k0} = 1 \quad \forall\ k$ is addressed in [18] (Corollary 1). The rest of the proof follows from the proof of Theorem 1. □

The numerical results of this control are illustrated in Sec. VI.

C. Time-Splay Circular Formation

In this section, a control algorithm is derived to stabilize a circular formation in which the temporal spacing between particles is regulated. Because all particles are traveling at unit speed relative to the flowfield, the spatial separation between particles may not be controllable. However, the temporal spacing between particles can be adjusted to ensure that any point along the vehicle's trajectory has a consistent revisit rate. A spatially uniform flowfield is assumed to be of the form $f(t) = \eta_0 e^{i\Omega t}$, in which the magnitude η_0 is constant and the direction $\phi(t) = \Omega t$ rotates at a constant rate Ω. (Such a flowfield arises in a reference frame fixed to a constant-speed target that turns at a constant rate.)

Equation (19) shows that $\nu_k = \omega_0 s_k(t)$ drives particle k in a fixed circle of radius $|\omega_0|^{-1}$. Consider the change of variables $\gamma_k' = \gamma_k - \Omega t$, which implies

$$\dot{\gamma}_k' = \dot{\gamma}_k - \Omega = \omega_0 s_k(t) - \Omega \tag{30}$$

Using Eq. (13), the following expression for $s_k(t)$ is obtained, which depends on γ_k' instead of time:

$$s_k(t) = s(\gamma_k') = \eta_0\cos\gamma_k' + \sqrt{(1 - \eta_0^2\sin^2\gamma_k')} \tag{31}$$

For the ensuing calculations to be nonsingular, it is required that Eq. (30) not have a fixed point, as ensured by the following lemma.

Lemma 1. Choosing

$$|\omega_0| > \frac{\operatorname{sgn}(\omega_0)\Omega}{1 - |\eta_0|} \quad \text{or} \quad |\omega_0| < \frac{\operatorname{sgn}(\omega_0)\Omega}{1 + |\eta_0|} \tag{32}$$

ensures that the equation does not have a fixed point.

Proof. Requiring $\omega_0 s_k(t) - \Omega \neq 0$ implies

$$\min_{\gamma_k'} s(\gamma_k') > \frac{\Omega}{\omega_0} \tag{33}$$

or

$$\max_{\gamma_k'} s(\gamma_k') < \frac{\Omega}{\omega_0} \tag{34}$$

The minimum of $s(\gamma_k')$ in Eq. (31) is $s(\gamma_k') = 1 - |\eta_0|$, which occurs at $\gamma_k' = \pi$ if $\eta_0 > 0$ and $\gamma_k' = 0$ if $\eta_0 < 0$. Substituting $s(\gamma_k') = 1 - |\eta_0|$ into Eq. (33) yields $|\omega_0| > \operatorname{sgn}(\omega_0)\Omega/(1 - |\eta_0|)$. The maximum of $s(\gamma_k')$ in Eq. (31) is $s(\gamma_k') = 1 + |\eta_0|$, which occurs at $\gamma_k' = 0$ if $\eta_0 > 0$ and $\gamma_k' = \pi$ if $\eta_0 < 0$. Substituting $s(\gamma_k') = 1 + |\eta_0|$ into Eq. (34) yields $\operatorname{sgn}(\omega_0)|\omega_0| < \Omega/(1 + |\eta_0|)$. Therefore, placing the conditions in Eq. (32) on $|\omega_0|$ ensures that Eq. (30) will not have a fixed point. □

Integrating Eq. (30) by separation of variables yields

$$t = \int_0^{\gamma_k'(t)} \frac{\mathrm{d}\gamma'}{\omega_0 s(\gamma') - \Omega} \tag{35}$$

A time-phase variable is introduced to regulate the time separation of the N particles [18]. The time phase for a time-varying uniform flow $f(t) = \eta_0 e^{i\Omega t}$ is

$$\psi_k \triangleq \frac{2\pi}{T}\int_0^{\gamma_k'(t)} \frac{\mathrm{d}\gamma'}{\omega_0 s(\gamma') - \Omega} \tag{36}$$

where the period of a single revolution T is

$$T = \int_0^{2\pi} \frac{\mathrm{d}\gamma'}{\omega_0 s(\gamma') - \Omega} \tag{37}$$

The time derivative of Eq. (36) is

$$\dot{\psi}_k = \frac{2\pi}{T}\frac{\nu_k - \Omega}{\omega_0 s_k(t) - \Omega} \tag{38}$$

Choosing ω_0 to satisfy Eq. (32) ensures $\dot{\psi}_k$ is nonsingular by Lemma 1. Note that Eq. (38) implies that the control $\nu_k = \omega_0 s_k(t)$ yields a constant time-phase rate, $\dot{\psi}_k = 2\pi/T$. To stabilize a circular formation in which the relative time phases are regulated, a phase potential is added to the Lyapunov function. The composite potential is [6]

$$V(\boldsymbol{r},\boldsymbol{\gamma}) = S(\boldsymbol{r},\boldsymbol{\gamma}) + \frac{T}{2\pi}U(\boldsymbol{\psi}) \tag{39}$$

The phase potential $U(\boldsymbol{\psi})$ is a smooth function satisfying the rotational symmetry property $U(\boldsymbol{\psi}+\psi_0\mathbf{1}) = U(\boldsymbol{\psi})$, which implies [6]

$$\sum_{k=1}^{N}\frac{\partial U}{\partial \psi_k} = 0 \tag{40}$$

Using Eqs. (38) and (40) gives the following time derivative of the potential Eq. (39):

$$\begin{aligned}\dot{V} &= \sum_{k=1}^{N}\langle e^{i\gamma_k}, P_k\boldsymbol{c}\rangle[s_k(t) - \omega_0^{-1}v_k] + \frac{T}{2\pi}\frac{\partial U}{\partial \psi_k}\dot{\psi}_k \\ &= \sum_{k=1}^{N}\left[s_k(t)\langle e^{i\gamma_k}, P_k\boldsymbol{c}\rangle - \frac{\partial U}{\partial \psi_k}\frac{\omega_0 s_k(t)}{\omega_0 s_k(t)-\Omega}\right]\left(\frac{\omega_0 s_k(t) - v_k}{\omega_0 s_k(t)}\right)\end{aligned} \tag{41}$$

The following theorem extends [18] (Theorem 5) to incorporate a spatially invariant time-varying flowfield.

Theorem 3. Let $f(t) = \eta_0 e^{i\Omega t}$ be a spatially invariant flowfield satisfying the condition $|\eta_0| < 1 \quad \forall\ t$. Also, let $U(\psi)$ be a smooth, rotationally symmetric phase potential. Choosing the control

$$v_k = \omega_0 s_k(t)\left[1 + K\left(s_k(t)\langle e^{i\gamma_k}, P_k\boldsymbol{c}\rangle - \frac{\partial U}{\partial \psi_k}\frac{\omega_0 s_k(t)}{\omega_0 s_k(t)-\Omega}\right)\right] \qquad K > 0 \tag{42}$$

where $\omega_0 \neq 0$, satisfies the constraint in Lemma 1, stabilizes a circular formation with radius $|\omega_0|^{-1}$ and a direction determined by the sign of ω_0, in which the time-phase arrangement is a critical point of $U(\boldsymbol{\psi})$.

Proof. Using the control in Eq. (42) with the potential in Eq. (41) yields

$$\begin{aligned}\dot{V} &= -K\sum_{k=1}^{N}\left\{[s_k(t)]^2\langle e^{i\gamma_k}, P_k\boldsymbol{c}\rangle^2 - 2\frac{\partial U}{\partial \psi_k}\frac{\omega_0 s_k(t)}{\omega_0 s_k(t)-\Omega}\langle e^{i\gamma_k}, P_k\boldsymbol{c}\rangle\right. \\ &\quad \left. + \left(\frac{\partial U}{\partial \psi_k}\frac{\omega_0 s_k(t)}{\omega_0 s_k(t)-\Omega}\right)^2\right\} = -K\sum_{k=1}^{N}\left[s_k(t)\langle e^{i\gamma_k}, P_k\boldsymbol{c}\rangle\right. \\ &\quad \left. - \left(\frac{\partial U}{\partial \psi_k}\frac{\omega_0 s_k(t)}{\omega_0 s_k(t)-\Omega}\right)\right]^2 \le 0\end{aligned} \tag{43}$$

By an invariancelike principle ([25], Theorem 8.4), the solutions of Eq. (4) converge to the set $\{\dot{V} = 0\}$ for which

$$s_k(t)\langle e^{i\gamma_k}, P_k\boldsymbol{c}\rangle - \frac{\partial U}{\partial \psi_k}\frac{\omega_0 s_k(t)}{\omega_0 s_k(t)-\Omega} = 0 \tag{44}$$

for $k = 1, \ldots, N$. By Eq. (42), in this set, $v_k = \omega_0 s_k(t)$. Thus each particle travels around a circle with a fixed center and radius $|\omega_0|^{-1}$. Also, $\dot{\psi}_k = 2\pi/T$, which implies that $U(\boldsymbol{\psi})$ is constant [by Eq. (40)] and $\partial U/\partial\psi_k = 0 \quad \forall\ k$. The constraint in Eq. (44) reduces to

$$\langle e^{i\gamma_k}, P_k\boldsymbol{c}\rangle = 0 \tag{45}$$

The rest of the proof follows the proof of Theorem 1. □

Theorem 3 establishes convergence to a critical point of a rotationally symmetric potential $U(\boldsymbol{\psi})$. As an example, consider a potential for which the minimum corresponds to a time-splay formation [18] in which all of the relative time phases between consecutive particles around the formation are equal to $2\pi/N$:

$$U^{(M,N)}(\boldsymbol{\psi}) = \sum_{m=1}^{M}K_m U_m \tag{46}$$

where

$$U_m(\boldsymbol{\psi}) = \frac{N}{2}|p_{m\psi}|^2; \qquad p_{m\psi} \triangleq \frac{1}{mN}\sum_{k=1}^{N}e^{im\psi_k}$$

renders the set of time-splay formations uniformly asymptotically stable, since they are the absolute minimum of $U^{(M,N)}$ when $M = N$. Note that $K_m > 0$ for $m = 1, \ldots, N-1$, and $K_N < 0$.

Figure 3 illustrates Theorem 3, showing $N = 5$ particles as they converge to a time-splay configuration for a time-varying spatially uniform flowfield of the form $f(t) = \eta_0 e^{i\Omega t}$. Setting parameters $\eta_0 = 0.5$ and $\Omega = 0.01$ and choosing $\omega_0 = 0.1$ ensures that the constraint in Lemma 1 is satisfied. Figure 3a shows the particles as they initially converge to a circle. Figure 3b shows the particles at time $t = 2000$ after they have converged to a circular formation and an equal temporal spacing. (The particles have unequal spatial separation, because they travel slower when moving against the flowfield and faster when moving with the flowfield.) The clustering of particles in the slower-speed region ensures equal temporal spacing. Figure 3c shows convergence of the relative time phases of sequential particles to $2\pi/N$, indicative of a time-splay configuration.

Introducing a virtual particle, as in the previous section, enables the center of the time-splay formation to be prescribed, as described in the following corollary.

Corollary 1. Let $f(t) = \eta_0 e^{i\Omega t}$ be a spatially invariant flowfield satisfying the condition $|\eta_0| < 1 \quad \forall\ t$. Also, let $U(\psi)$ be a smooth, rotationally symmetric phase potential. Choosing the control

$$\begin{aligned}v_k = \omega_0 s_k(t)\left\{1 + K\left[s_k(t)(\langle e^{i\gamma_k}, P_k\boldsymbol{c}\rangle + a_{k0}\langle e^{i\gamma_k}, c_k - c_0\rangle)\right.\right. \\ \left.\left. - \frac{\partial U}{\partial \psi_k}\frac{\omega_0 s_k(t)}{\omega_0 s_k(t)-\Omega}\right]\right\}; \qquad K > 0\end{aligned} \tag{47}$$

where $\omega_0 \neq 0$ satisfies the constraint in Lemma 1 and $a_{k0} = 1$ for at least one $k \in 1, \ldots, N$, and zero otherwise, stabilizes the set of circular formations centered on c_0 with radius $|\omega_0|^{-1}$ and a direction

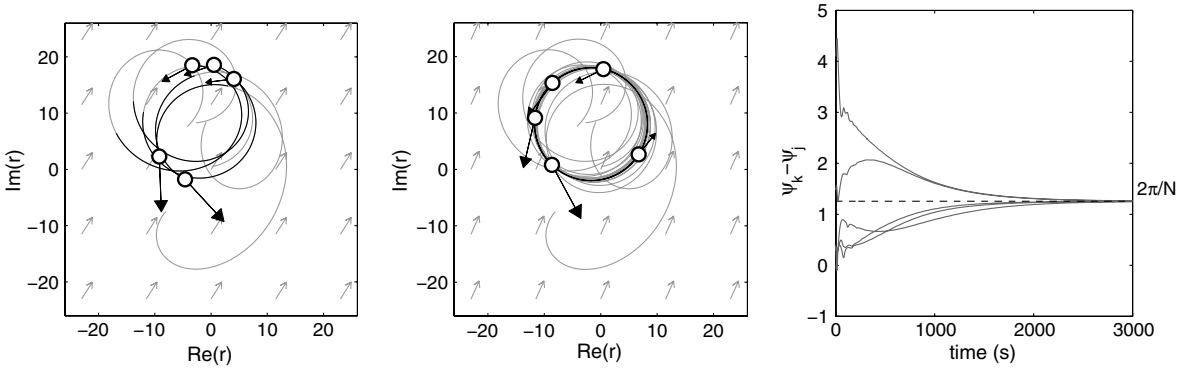

a) t = 100 s **b) t = 2000 s** **c) Relative time-phases**

Fig. 3 Stabilization of a time-splay formation with an arbitrary center in a time-varying spatially uniform flowfield.

determined by the sign of ω_0, in which the time-phase arrangement is a critical point of $U(\boldsymbol{\psi})$.

IV. Stabilization of a Circular Formation in an Estimated Flowfield

This section introduces control laws that stabilize a circular formation in an estimated uniform flowfield for which the direction may be rotating in time. Sections IV.A and IV.B present methods to stabilize circular formations with an arbitrary or prescribed center point in a uniform time-invariant flowfield. In Sec. IV.C, a time-splay formation is stabilized in a uniform, rotating flow. It is assumed that each particle knows its measured position r_k and orientation θ_k, although a dynamic estimate of position $\hat{r}_k$ is used to estimate the flow.

With the estimated flow, $\hat{f}_k(t) = \hat{f}(t, r_k)$, the estimated inertial velocity obeys

$$\dot{\hat{r}}_k = \hat{s}_k(t)e^{i\hat{\gamma}_k}; \qquad \dot{\hat{\gamma}}_k = \nu_k \tag{48}$$

where $\hat{s}_k(t)$ and $\hat{\gamma}_k$ are the magnitude and phase, respectively, of the estimated inertial velocity for particle k.

A. Circular Formation with an Arbitrary Center

In this section, a control law is developed to drive particles in a circular formation about an arbitrary, fixed point in the presence of an estimated, uniform, time-invariant flowfield. The control law works by dynamically estimating the flow and using the estimate in the control law.

Let $e_{1,k} = \hat{r}_k - r_k$ and $e_{2,k} = \hat{f}_k - f_k$ denote the estimation errors for particle k. Consider the estimator dynamics

$$\dot{\hat{r}}_k = e^{i\theta_k} + \hat{f}_k - K_1(\hat{r}_k - r_k); \qquad \dot{\hat{f}}_k = -K_2(\hat{r}_k - r_k) \tag{49}$$

This yields

$$\dot{e}_{1,k} = e^{i\theta_k} + \hat{f}_k - K_1(\hat{r}_k - r_k) - e^{i\theta_k} - f_k = -K_1 e_{1,k} + e_{2,k}$$
$$\dot{e}_{2,k} = -K_2(\hat{r}_k - r_k) = -K_2 e_{1,k}$$

In matrix form, the estimator dynamics for particle k are

$$\begin{bmatrix} \dot{e}_{1,k} \\ \dot{e}_{2,k} \end{bmatrix} = \underbrace{\begin{bmatrix} -K_1 & 1 \\ -K_2 & 0 \end{bmatrix}}_{\triangleq A} \begin{bmatrix} e_{1,k} \\ e_{2,k} \end{bmatrix} \tag{50}$$

Lemma 2. Choosing gains $K_2 > 0$ and $K_1 = 2\sqrt{K_2} > 0$ in the error dynamics of Eq. (50) exponentially stabilizes the origin $e_{1,k} = e_{2,k} = 0 \quad \forall\ k$.

Proof. The eigenvalues of A are $\lambda = (-K_1 \pm \sqrt{K_1^2 - 4K_2})/2$. Choosing $K_1 = 2\sqrt{K_2}$ results in $\lambda = -K_1$ with multiplicity two. □

The following is a result of Lemma 2.

Lemma 3. The matrix A defined in Eq. (50) is negative definite, and the quadratic form

$$Q_k(A) = \begin{bmatrix} e_{1,k} & e_{2,k} \end{bmatrix} \begin{bmatrix} -K_1 & 1 \\ -K_2 & 0 \end{bmatrix} \begin{bmatrix} e_{1,k} \\ e_{2,k} \end{bmatrix}$$
$$= -K_1 e_{1,k}^2 - K_2 e_{1,k} e_{2,k} + e_{1,k} e_{2,k} \le 0 \tag{51}$$

is equal to zero only when $e_{1,k} = e_{2,k} = 0$ for $k \in \{1, \ldots, N\}$.

Let $\hat{c}_k$ be the estimated center,

$$\hat{c}_k = \hat{r}_k + \omega_0^{-1} i e^{i\hat{\gamma}_k} \tag{52}$$

and consider the candidate Lyapunov function

$$\hat{S}(\hat{\boldsymbol{r}}, \hat{\boldsymbol{\gamma}}) \triangleq \tfrac{1}{2}\langle \hat{\boldsymbol{c}}, P\hat{\boldsymbol{c}} \rangle + \tfrac{1}{2}(\|\boldsymbol{e}_1\|^2 + \|\boldsymbol{e}_2\|^2) \tag{53}$$

where $\boldsymbol{e}_1 = [e_{1,1}, e_{1,2}, \ldots, e_{1,N}]^T$, $\boldsymbol{e}_2 = [e_{2,1}, e_{2,2}, \ldots, e_{2,N}]^T$, and $\hat{\boldsymbol{c}}$ is the vector of center points defined by Eq. (52). $\hat{S}$ is equal to zero when $\hat{\boldsymbol{c}} = c_0\mathbf{1}$, $c_0 \in \mathbb{C}$, and all estimation errors are zero. The time derivative of $\hat{S}$ along the solutions of Eqs. (48) and (50) is

$$\dot{\hat{S}} = \sum_{k=1}^{N} (\langle \dot{\hat{c}}_k, P_k\hat{\boldsymbol{c}} \rangle + \dot{e}_{1,k} e_{1,k} + \dot{e}_{2,k} e_{2,k}) = \sum_{k=1}^{N} \Big[\langle e^{i\hat{\gamma}_k}, P_k\hat{\boldsymbol{c}} \rangle [\hat{s}_k(t) - \omega_0^{-1}\nu_k] + \underbrace{e_{1,k}(-K_1 e_{1,k} + e_{2,k}) + e_{2,k}(-K_2 e_{1,k})}_{=Q_k(A)} \Big] \tag{54}$$

The following theorem extends Theorem 1 to the case of an estimated, uniform, time-invariant flowfield.

Theorem 4. Let $f_k(t) = \beta \in \mathbb{R}$, where $|\beta| < 1$ is an unknown time-invariant flowfield. Also, let $\hat{r}_k$ and $\hat{f}_k$ evolve according to Eq. (49) with $K_2 > 0$ and $K_1 = 2\sqrt{K_2}$. Choosing the control

$$\nu_k = \omega_0[\hat{s}_k(t) + K\langle P_k\hat{\boldsymbol{c}}, e^{i\hat{\gamma}_k} \rangle]; \qquad K > 0 \tag{55}$$

forces convergence of solutions of the model in Eq. (48) to the set of a circular formations with radius $|\omega_0|^{-1}$ and a direction determined by the sign of ω_0.

Proof. Substituting Eq. (55) into Eq. (54) shows that the time derivative of the potential $\hat{S}(\hat{\boldsymbol{r}}, \hat{\boldsymbol{\gamma}})$ satisfies

$$\dot{\hat{S}} = \sum_{k=1}^{N} [-K\langle P_k\hat{\boldsymbol{c}}, e^{i\hat{\gamma}_k} \rangle^2 + Q_k(A)] \le 0 \tag{56}$$

Using the invariance principle, all of the solutions of Eq. (4) with the controller in Eq. (55) converge to the largest invariant set, where

$$-K\langle P_k\hat{\boldsymbol{c}}, e^{i\hat{\gamma}_k} \rangle^2 + Q_k(A) = 0 \quad \forall\ k \tag{57}$$

By Lemma 3, the condition in Eq. (57) is satisfied only when both $Q_k(A) = 0$ and $\langle P_k\hat{\boldsymbol{c}}, e^{i\hat{\gamma}_k} \rangle = 0$ independently. $Q_k(A) = 0$ implies that the estimated values $\hat{r}_k$ and $\hat{f}_k$ equal the measured values r_k and f_k. Values $\hat{\gamma}_k$ and $\hat{s}_k(t)$ are functions of $\hat{f}_k$ and θ_k. This implies that $\hat{\gamma}_k$ and $\hat{s}_k(t)$ approach their measured values and, by Eq. (52), $\hat{c}_k$ converges to c_k. The condition, $\langle P_k\hat{\boldsymbol{c}}, e^{i\hat{\gamma}_k} \rangle = 0$ is satisfied for all k only when $P_k\hat{\boldsymbol{c}}$ is constant and equal to zero. Since the null space of P is spanned by $\mathbf{1}$, this implies $\hat{c}_k = \hat{c}_j \quad \forall\ k, j$. In this set, the control in Eq. (55) evaluates to $\nu_k = \omega_0\hat{s}_k(t)$ and $\dot{\hat{c}}_k = 0$, which implies that each particle converges to circular motion around the same fixed center. □

B. Circular Formation with a Prescribed Center

Under the control in Eq. (55), the center of the circular formation depends only on the initial conditions of the particles and the flowfield. As with the case of the known flowfield, introducing a symmetry-breaking virtual particle (indexed by $k = 0$) will prescribe a center point for the formation. Consider the augmented potential $\tilde{S}(\hat{\boldsymbol{r}}, \hat{\boldsymbol{\gamma}}) = \hat{S}(\hat{\boldsymbol{r}}, \hat{\boldsymbol{\gamma}}) + S_0(\hat{\boldsymbol{r}}, \hat{\boldsymbol{\gamma}})$, where

$$S_0(\hat{\boldsymbol{r}}, \hat{\boldsymbol{\gamma}}) = \frac{1}{2}\sum_{j=1}^{N} a_{j0}|\hat{c}_j - c_0|^2 \tag{58}$$

and $\hat{c}_k$ is defined by Eq. (52). Taking the time derivative of Eq. (58) along the solutions of Eqs. (48) and (50) gives

$$\dot{\tilde{S}} = \sum_{j=1}^{N} \Big[(\langle e^{i\hat{\gamma}_j}, P_j\hat{\boldsymbol{c}} \rangle + a_{j0}\langle e^{i\hat{\gamma}_j}, \hat{c}_j - c_0 \rangle)[\hat{s}_j(t) - \omega_0^{-1}\nu_j] + \underbrace{e_{1,j}(-K_1 e_{1,j} + e_{2,j}) + e_{2,j}(-K_2 e_{1,j})}_{=Q_j(A)} \Big] \tag{59}$$

Theorem 5. Let $f_k(t) = \beta \in \mathbb{R}$, where $|\beta| < 1$ is an unknown time-invariant flow. Also, let $\hat{r}_k$ and $\hat{f}_k$ evolve according to Eq. (49) with $K_2 > 0$ and $K_1 = 2\sqrt{K_2}$. Choosing the control

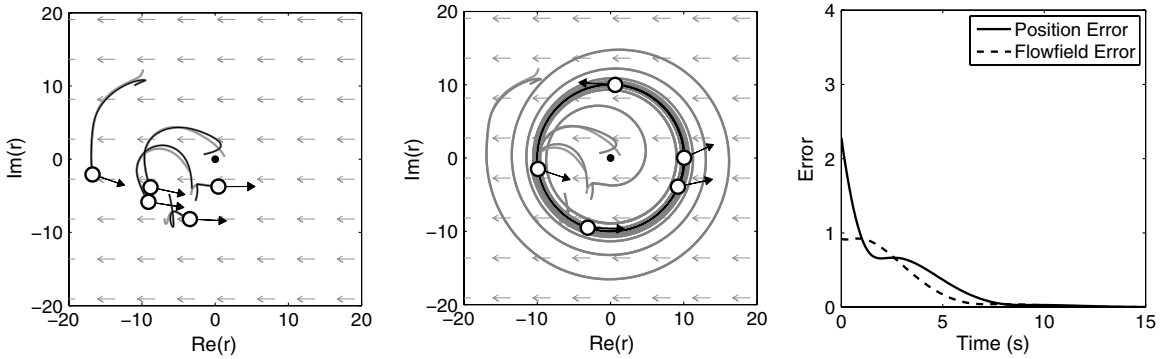

a) t = 20 s **b) t = 1000 s** **c) Error dynamics, k = 3**

Fig. 4 Stabilization of circular formation in uniform flowfield $f = -0.8$ with a prescribed center point $c_0 = 0$.

$$v_k = \omega_0[\hat{s}_k(t) + K(\langle e^{i\hat{\gamma}_k}, P_k\hat{\boldsymbol{c}}\rangle + a_{k0}\langle e^{i\hat{\gamma}_k}, \hat{c}_k - c_0\rangle)]; \qquad K > 0 \tag{60}$$

forces convergence of the solutions of the model in Eq. (48) to the set of circular formations centered at c_0 with radius $|\omega_0|^{-1}$ and direction determined by the sign of ω_0.

The proof of this theorem is omitted for brevity.

Figure 4 illustrates Theorem 5 with estimator gains $K_2 = 0.2$ and $K_1 = 2\sqrt{K_2} = 0.894$ and a uniform flowfield $f = -0.8$. Figures 4a and 4b show tracks of the estimated (darker track) and actual (lighter track) particle positions at 20 and 1000 s, respectively, as they converge to a circular formation about the prescribed center point, $c_0 = 0$. Figure 4c shows convergence to zero of estimator errors in the position and the flow for particle $k = 3$.

C. Time-Splay Formation with a Rotating Flowfield

In this section, a control law is derived to stabilize particles to a time-splay formation in an estimated, spatially invariant, rotating flowfield. (A rotating flowfield is defined to be a uniform flowfield for which the direction is rotating in time.) Without speed control, it may not be possible to regulate the spatial separation of particles, but it is possible to regulate the temporal separation in an estimated flowfield, as shown next.

Given a uniform time-varying flowfield $f(t) = \eta_0 e^{i\Omega t}$, choose $e_{1,k} = \hat{r}_k - r_k$ and $e_{2,k} = \hat{f}_k(t) - f_k(t)$. The rotational rate Ω is assumed to be known; the flow speed η_0 and initial orientation are unknown. Consider the estimator dynamics

$$\begin{aligned}\dot{\hat{r}}_k &= e^{i\theta_k} + \hat{f}_k(t) - K_1(\hat{r}_k - r_k)\\ \dot{\hat{f}}_k &= -K_2(\hat{r}_k - r_k) + \Omega i\hat{f}_k(t)\end{aligned} \tag{61}$$

Taking the derivative of the error and plugging in Eq. (61) yields

$$\dot{e}_{1,k} = e^{i\theta_k} + \hat{f}_k - K_1(\hat{r}_k - r_k) - e^{i\theta_k} - f_k(t) = -K_1 e_{1,k} + e_{2,k}$$
$$\dot{e}_{2,k} = -K_2 e_{1,k} + \Omega i e_{2,k}$$

The estimator dynamics for particle k are

$$\begin{bmatrix}\dot{e}_{1,k}\\ \dot{e}_{2,k}\end{bmatrix} = \underbrace{\begin{bmatrix}-K_1 & 1\\ -K_2 & \Omega i\end{bmatrix}}_{\triangleq B}\begin{bmatrix}e_{1,k}\\ e_{2,k}\end{bmatrix} \tag{62}$$

Lemma 4. Choosing gains $K_1 > |\Omega|$ and $K_2 = (K_1^2 - \Omega^2)/4$ in the error dynamics of Eq. (62) that exponentially stabilize the origin $e_{1,k} = e_{2,k} = 0$ for $k = [1, \ldots, N]$.

Proof. The real parts of the eigenvalues of B (see Appendix A) are

$$Re(\lambda) = \frac{-K_1}{2} \pm \frac{\sqrt{\sqrt{(K_1^2 - \Omega^2 - 4K_2)^2 + 4K_1^2\Omega^2} + (K_1^2 - \Omega^2 - 4K_2)}}{2\sqrt{2}} \tag{63}$$

Letting $K_1 > |\Omega|$ and $K_2 = (K_1^2 - \Omega^2)/4$ result in $Re(\lambda) = (-K_1 \pm \sqrt{K_1\Omega})/2$. $K_1 > |\Omega|$, which implies $Re(\lambda) < 0$. □

The following result is a consequence of Lemma 4.

Lemma 5. Matrix B, defined in Eq. (62), is negative definite, and the quadratic form

$$Q_k(B) \triangleq \begin{bmatrix}e_{1,k} & e_{2,k}\end{bmatrix}\begin{bmatrix}-K_1 & 1\\ -K_2 & \Omega i\end{bmatrix}\begin{bmatrix}e_{1,k}\\ e_{2,k}\end{bmatrix} = -K_1 e_{1,k}^2 - K_2 e_{1,k}e_{2,k} + e_{1,k}e_{2,k} + \Omega i e_{2,k}^2 \le 0 \tag{64}$$

is only equal to zero when $e_{1,k} = e_{2,k} = 0 \quad \forall\ k$.

The estimator dynamics in Eq. (62) are used to stabilize a time-splay formation for a flowfield with a known rotation rate $\Omega(t)$. Consider the Lyapunov function

$$\hat{V}(\hat{\boldsymbol{r}}, \hat{\boldsymbol{\gamma}}) = \frac{1}{2}\langle\hat{\boldsymbol{c}}, P\hat{\boldsymbol{c}}\rangle + \frac{T}{2\pi}U(\hat{\boldsymbol{\psi}}) + \frac{1}{2}(\|\boldsymbol{e}_1\|^2 + \|\boldsymbol{e}_2\|^2) \tag{65}$$

where $\hat{\boldsymbol{c}}$ is the vector of estimated center points defined by Eq. (52). Taking the time derivative along solutions of Eqs. (48) and (62) yields

$$\dot{\hat{V}} = \sum_{k=1}^{N}\Bigg[\left(\hat{s}_k(t)\langle e^{i\hat{\gamma}_k}, P_k\hat{\boldsymbol{c}}\rangle - \frac{\partial U}{\partial\hat{\psi}_k}\frac{\omega_0\hat{s}_k(t)}{\omega_0\hat{s}_k(t) - \Omega}\right)\left(\frac{\omega_0\hat{s}_k(t) - v_k}{\omega_0\hat{s}_k(t)}\right) + \underbrace{e_{1,k}(-K_1e_{1,k} + e_{2,k}) + e_{2,k}(-K_2e_{1,k} + \Omega i e_{2,k})}_{=Q_k(B)}\Bigg] \tag{66}$$

The following result extends Theorem 3 to incorporate an estimated, spatially invariant, rotating flow.

Theorem 6. Let $f(t) = \eta_0 e^{i\Omega t}$ be an unknown spatially invariant flowfield satisfying the condition $|\eta_0| < 1 \quad \forall\ t$. Also, let $U(\hat{\boldsymbol{\psi}})$ be a smooth, rotationally symmetric phase potential. Let $\hat{r}_k$ and $\hat{f}_k$ evolve according to Eq. (61) with $K_1 > |\Omega|$ and $K_2 = (K_1^2 - \Omega^2)/4$. Choosing the control

$$v_k = \omega_0\hat{s}_k(t)\left[1 + K\left(\hat{s}_k(t)\langle e^{i\hat{\gamma}_k}, P_k\hat{\boldsymbol{c}}\rangle - \frac{\partial U}{\partial\hat{\psi}_k}\frac{\omega_0\hat{s}_k(t)}{\omega_0\hat{s}_k(t) - \Omega}\right)\right] \qquad K > 0 \tag{67}$$

where $\omega_0 \neq 0$ satisfies the constraint in Lemma 1, stabilizes the set of circular formations with radius $|\omega_0|^{-1}$ and the direction determined by the sign of ω_0, in which the time-phase arrangement is a critical point of $U(\hat{\boldsymbol{\psi}})$.

Proof. Using the control in Eq. (67) with the potential in Eq. (66) yields

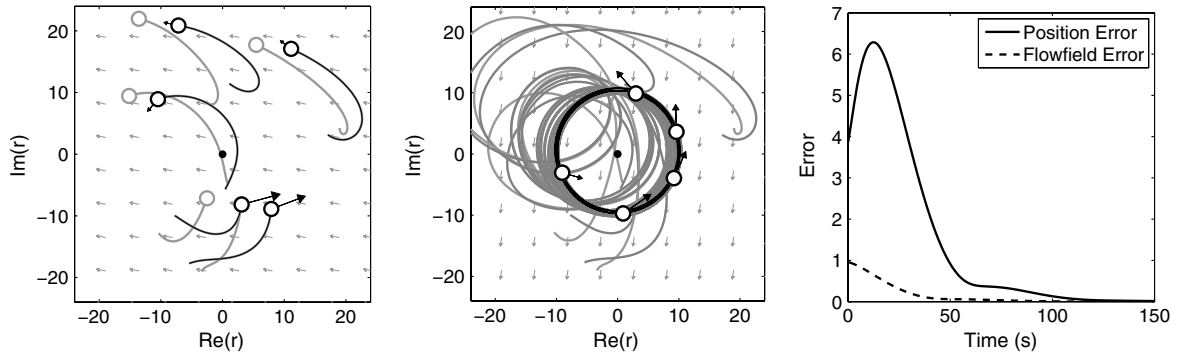

a) $t = 20$ s **b) $t = 3000$ s** **c) Error dynamics, $k = 3$**

Fig. 5 Stabilization of a circular time-splay formation centered at $c_0 = 0$ in an estimated rotating flowfield, $f(t) = \eta_0 e^{i\Omega t}$, with $\eta_0 = 0.5$ and $\Omega = -0.01$.

$$\dot{\hat{V}} = \sum_{k=1}^{N} \left\{ -K \left[\hat{s}_k(t) \langle e^{i\hat{\gamma}_k}, P_k \hat{\boldsymbol{c}} \rangle - \left(\frac{\partial U}{\partial \hat{\psi}_k} \frac{\omega_0 \hat{s}_k(t)}{\omega_0 \hat{s}_k(t) - \Omega} \right) \right]^2 + Q_k(B) \right\} \leq 0$$

By an invariancelike principle ([25], Theorem 8.4), the solutions of Eq. (4) converge to the set $\{\dot{\hat{V}} = 0\}$ for which

$$-K \left(\hat{s}_k(t) \langle e^{i\hat{\gamma}_k}, P_k \hat{\boldsymbol{c}} \rangle - \frac{\partial U}{\partial \hat{\psi}_k} \frac{\omega_0 \hat{s}_k(t)}{\omega_0 \hat{s}_k(t) - \Omega} \right)^2 + Q_k(B) = 0, \quad \forall\ k \tag{68}$$

According to Lemma 5, both terms in Eq. (68) must equal zero and $Q_k(B) = 0$ only when the estimated $\hat{r}_k$ and $\hat{f}_k$ values have converged to their corresponding measured values. The convergence of these estimated values along with the known value θ_k also implies that $\hat{s}_k(t)$, $\hat{\gamma}_k$, and $\hat{c}_k$ converge to their measured values. The rest of the proof follows from the proofs of Theorems 3 and 4. □

Figure 5 illustrates Theorem 6. The simulation uses estimator gains $K_1 = 0.1$ and $K_2 = (K_1^2 - \Omega^2)/4$. The rotating flowfield parameters are $\eta = 0.5$, $\Omega = -0.01$, and $\omega_0 = .1$, which satisfy Lemma 1. Figures 5a and 5b show tracks of the estimated (darker track) and actual (lighter track) particle positions at 20 and 3000 s, respectively, as they converge to a time-splay formation about the prescribed center point, $c_0 = 0$. Figure 5c shows convergence of the estimator errors to zero for a single particle, $k = 3$. The initial conditions for all particles are set randomly. In this simulation, the initial estimated flowfield for particle $k = 3$ started in the opposite direction as the actual flowfield causing the measured and estimated positions to temporarily diverge, as seen by the peak in Fig. 5c.

V. Motion Coordination with a Turn-Rate Constraint

Physical restrictions on an autonomous vehicle often constrain the turn-rate control that may be applied to a system. In UAVs, a turn-rate constraint can result from the aircraft's maximum bank angle [26]. In the previous sections, this bound was relaxed, allowing for potentially unlimited turn-rate control. In this section, it is shown that the previous results are valid even when there is a turn-rate constraint; the constraint imposes a lower bound on the feasible radius of a circular formation in a flowfield.

In terms of the inertial speed $s_k(t)$ and orientation γ_k, the model in Eq. (1) is equivalent to

$$\dot{r}_k = s_k(t) e^{i\gamma_k}; \qquad \dot{\gamma}_k = \text{sat}(\nu_k; \nu_{\max}) \tag{69}$$

where $\nu_{\max} \triangleq \nu_k(u_{\max})$ is a constraint on the steering control induced by the saturation on u_k. The relationship between $\nu_{\max}$ and $u_{\max}$ is defined in Sec. V.A for a uniform time-invariant flowfield and in Sec. V.B for a uniform, rotating flowfield.

A. Turn-Rate Constraint in a Uniform Time-Invariant Flowfield

The following result establishes the maximum required turn rate for a particle to travel in a circle about a fixed center in a uniform time-invariant flowfield. (Because of the flow, the turn rate changes as the particle travels around the circle.)

Lemma 6. Consider the circular motion with radius $|\omega_0|^{-1}$ of a particle in a steady flow $f_k = \beta \in \mathbb{R}$. The maximum required turn rate is

$$u_{\max} \triangleq \max_{\gamma_k} u(\gamma_k) = |\omega_0|(1 + |\beta|)^2 > 0 \tag{70}$$

The maximum steering control is

$$\nu_{\max} \triangleq \nu(u_{\max}) = |\omega_0|(1 + |\beta|) \tag{71}$$

Proof. Consider the particle model in Eq. (1). For a uniform time-invariant flowfield β, the turn-rate control u_k can be determined from Eq. (14) to be

$$u_k = \frac{\nu_k}{1 - \beta s_k^{-1}(t) \cos \gamma_k} \tag{72}$$

Given a circular control $\nu_k = \omega_0 s_k(t)$ with inertial speed

$$s_k(t) = \beta \cos \gamma_k + (1 - \beta^2 \sin^2 \gamma_k)^{1/2} \tag{73}$$

the turn rate in Eq. (72) is

$$u_k = u(\gamma_k) = \frac{\omega_0 [\beta \cos \gamma_k + (1 - \beta^2 \sin^2 \gamma_k)^{1/2}]^2}{(1 - \beta^2 \sin^2 \gamma_k)^{1/2}} \tag{74}$$

The maximum turn rate

$$u_{\max} = \max_{\gamma_k} u(\gamma_k) = |\omega_0|(1 + |\beta|)^2 \tag{75}$$

occurs when $\sin \gamma_k = 0$ and $\beta \cos \gamma_k = |\beta|$; that is, $\gamma_k = 0$ if $\beta < 0$ or $\gamma_k = \pi$ if $\beta > 0$. Under these conditions, Eq. (73) becomes $s_k(t) = 1 + |\beta|$. The controller ν_k is bounded through its relationship to $u_{\max}$. Substituting $s_k(t) = 1 + |\beta|$ and Eq. (75) into Eq. (72) gives

$$\nu_{\max} \triangleq \nu(u_{\max}) = \frac{u_{\max}}{(1 + |\beta|)^2} = |\omega_0|(1 + |\beta|) \tag{76}$$

□

Figure 6a shows the maximum turn rate $u_{\max}$ as a function of the formation radius $|\omega_0|^{-1}$ for $\beta = 0.75$. (The maximum turn rate is the value necessary to maintain a circular formation of radius $|\omega_0|^{-1}$ given a spatially uniform flow β.) Figure 6b plots the turn rate for a single particle initialized with a random position and velocity as it converges under control $\nu_k = \omega_0 s_k(t)$ to a circle of radius $|\omega_0|^{-1} = 10$. Note that the particle stays at or below the maximum turn rate as it maintains a circle of the prescribed radius. The following result shows that, even if the steering control is saturated, the circular-formation control law is still justified.

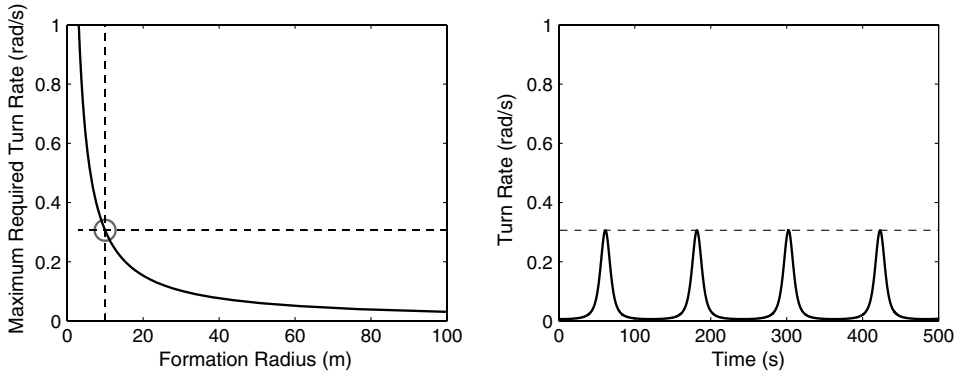

Fig. 6 Turn rate shown as a function of a) formation radius and b) time for a particle on a circle of radius $|\omega_0|^{-1} = 10$ in flow $\beta = 0.75$.

Theorem 7. Consider the model in Eq. (69) with $f_k = \beta \in \mathbb{R}$, $u_{\max} > 0$, and $\nu_{\max} = \nu_k(u_{\max})$. If ω_0 satisfies

$$|\omega_0| < \frac{u_{\max}}{(1 + |\beta|)^2} \tag{77}$$

then the control in Eq. (23) forces convergence of all particles to the set of circular formations with radius $|\omega_0|^{-1}$ and the direction determined by the sign of ω_0.

Proof. Consider the Lyapunov function

$$V = \tfrac{1}{2}\langle \boldsymbol{c}, P\boldsymbol{c}\rangle \tag{78}$$

The time derivative of V along the solutions of Eq. (69) is

$$\dot{V} = \sum_{k=1}^{N} \langle P_k \boldsymbol{c}, e^{i\gamma_k}\rangle [s_k(t) - \omega_0^{-1}\nu_k] \tag{79}$$

Using the control in Eq. (23), observe that

$$\langle e^{i\gamma_k}, P_k \boldsymbol{c}\rangle = \frac{\nu_k - s_k(t)\omega_0}{K\omega_0} \tag{80}$$

which implies

$$\begin{aligned}\dot{V} &= -\sum_{k=1}^{N} \frac{[s_k(t) - \omega_0^{-1}\nu_k]^2}{K} \\ &= -\frac{1}{K\omega_0^2}\sum_{k=1}^{N} \frac{[\omega_0 s_k(t) - \nu_k]^2}{K} \le 0 \quad \forall\ \nu_k\end{aligned} \tag{81}$$

When $-\nu_{\max} \le \nu_k \le \nu_{\max}$, $\dot{V} \le 0$; otherwise, $\dot{V}$ is strictly less than zero. Applying the invariance principle, the solutions of Eq. (4) converge to the largest invariant set for which

$$\langle P_k \boldsymbol{c}, e^{i\gamma_k}\rangle = 0 \tag{82}$$

In this set, Eq. (23) evaluates to $\nu_k = s_k(t)\omega_0$ and $\dot{c_k} = 0$, which implies that the particles travel in a circle with a fixed center. $P_k\boldsymbol{c}$ is constant and must evaluate to zero. Because P is spanned by $\mathbf{1}$, this condition is only satisfied when $P\boldsymbol{c} = 0$, which implies $c_k = c_j \quad \forall\ k, j$. The formation radius in Eq. (77) satisfies Eq. (75) in Lemma 6, ensuring that the control will drive all particles to a set of asymptotically stable circular formations with radius $|\omega_0|^{-1}$. □

By introducing a virtual particle, as was done in Theorem 2, one can similarly establish stabilization of a circular formation with a bounded turn rate at a prescribed center point.

Corollary 2. Consider the model in Eq. (69), where $f_k = \beta \in \mathbb{R}$, $u_{\max} > 0$, and $\nu_{\max} = \nu_k(u_{\max})$. If ω_0 satisfies

$$|\omega_0| < \frac{u_{\max}}{(1 + |\beta|)^2} \tag{83}$$

then the control in Eq. (27) forces convergence to the set of circular formations centered on c_0 with radius $|\omega_0|^{-1}$ and the direction determined by the sign of ω_0.

Figure 7 compares a system of particles that conform to the $u_{\max}$ constraint in Eq. (75) with one that does not. By violating Eq. (75), the particles do not have the turn-rate control necessary to maintain a circular formation of the chosen radius. This is illustrated in Fig. 7a using a bound of $u_{\max} = 0.1$. The particles fail to maintain a circular radius of $|\omega_0|^{-1} = 10$; that is, the solution does not converge to a circular formation. Figure 7b shows convergence to a circular formation with radius $|\omega_0|^{-1} = 30.6$, the smallest permissible radius for $u_{\max} = 0.1$, according to Corollary 2.

B. Turn-Rate Constraint in a Uniform, Rotating Flowfield

This section shows that the previous results hold for a spatially invariant, rotating flow, $f(t) = \eta_0 e^{i\Omega t}$.

Lemma 7. Consider the circular motion of a particle with radius $|\omega_0|^{-1}$ and flowfield $f(t) = \eta_0 e^{i\Omega t}$. The maximum turn rate of the particle required to maintain a circular formation is

$$u_{\max} \triangleq \max_{\gamma_k} u(\gamma_k) = \begin{cases} |\omega_0|(1 + |\eta_0|)^2 - |\eta_0||\Omega| & \text{if } 2|\omega_0| > |\Omega| \\ |\omega_0|(1 - |\eta_0|)^2 + |\eta_0||\Omega| & \text{if } 2|\omega_0| \le |\Omega| \end{cases} \tag{84}$$

The maximum steering control is

$$\nu_{\max} \triangleq \nu(u_{\max}) = \begin{cases} |\omega_0|(1 + |\eta_0|) & \text{if } 2|\omega_0| > |\Omega| \\ |\omega_0|(1 - |\eta_0|) & \text{otherwise} \end{cases} \tag{85}$$

Proof. From Eq. (14), it is seen that the turn-rate control u_k for a particle with the dynamics in Eq. (1) in a rotating flowfield, $f(t) = \eta_0 e^{i\Omega t}$, is

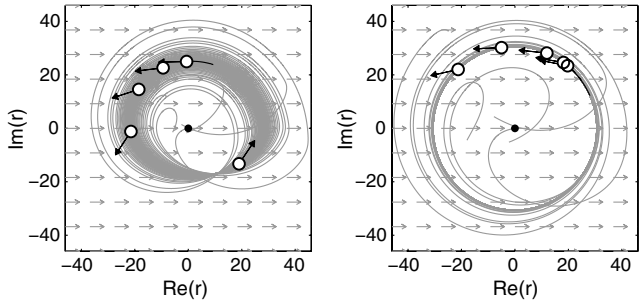

Fig. 7 Effects of a bounded turning control, $u_{\max} = 0.35$, in a spatially uniform flowfield with $\beta = 0.75$: a) circular formation unobtainable with radius $|\omega_0|^{-1} = 10$ and b) stable circular formation with radius $|\omega_0|^{-1} = 30.6$.

$$u_k = u(\gamma_k') = \frac{s_k(t)\nu_k - \Omega\eta_0\cos(\gamma_k')}{s_k(t) - \eta_0\cos(\gamma_k')} \tag{86}$$

where $\gamma_k' = \gamma_k - \Omega t$. The inertial speed $s_k(t)$ is determined by Eq. (13):

$$s_k(t) = s(\gamma_k') = \eta_0\cos(\gamma_k') + [1 - \eta_0^2\sin(\gamma_k')^2]^{1/2} \tag{87}$$

Substituting the circular control $\nu_k = \omega_0 s_k(t)$ into Eq. (86) and finding the extrema with respect to γ_k' yields critical points at $\gamma_k' = 0$ and $\gamma_k' = \pi$, which implies

$$u_k(0) = \omega_0(1+\eta_0)^2 - \eta_0\Omega \tag{88}$$

and

$$u_k(\pi) = \omega_0(1-\eta_0)^2 + \eta_0\Omega \tag{89}$$

Either Eq. (88) or Eq. (89) is a maximum point depending on the values of η_0, Ω, and ω_0. If $\eta_0 > 0$, then $u_k(0) > u_k(\pi)$ when $2\omega_0 > \Omega$. If $\eta_0 < 0$, then $u_k(0) > u_k(\pi)$ when $2\omega_0 < \Omega$, leading to Eq. (84). Under these conditions, Eq. (87) becomes $s_k(t) = 1 \pm |\eta|$, and substituting $s_k(t)$ and Eq. (84) into Eq. (86) gives Eq. (85). □

Theorem 8. Consider the model in Eq. (69) with $f(t) = \eta_0 e^{i\Omega t}$, $|\eta_0| < 1 \quad \forall\ t$, and $u_{\max} > 0$. If ω_0 satisfies

$$\begin{aligned} |\omega_0| &< (u_{\max} + |\eta_0||\Omega|)/(1+|\eta_0|)^2 \quad \text{if} \quad 2|\omega_0| > |\Omega| \\ |\omega_0| &< (u_{\max} - |\eta_0||\Omega|)/(1-|\eta_0|)^2 \quad \text{if} \quad 2|\omega_0| \le |\Omega| \end{aligned} \tag{90}$$

then the control in Eq. (23), with $\nu_{\max}$ given by Eq. (85), forces uniform convergence of the solutions to the model in Eq. (69) to the set of circular formations with radius $|\omega_0|^{-1}$ and the direction determined by the sign of ω_0.

The proof of Theorem 8 follows the proof of Theorem 7. Since $f(t)$ is time-varying, uniform asymptotic stability is established by the invariancelike principle, as in Theorem 1. The following theorem shows that stabilization of a time-splay formation is possible even with a bounded turn rate, thereby extending Theorem 3.

Theorem 9. Consider the model in Eq. (69) with the spatially invariant, rotating flowfield, $f = \eta_0 e^{i\Omega t}$ and $|\eta_0| < 1 \quad \forall\ t$. Also, let $U(\psi)$ be a smooth, rotationally symmetric phase potential, with ω_0 such that it satisfies both the constraint in Lemma 1 and

$$\begin{aligned} |\omega_0| &< (u_{\max} + |\eta_0||\Omega|)/(1+|\eta_0|)^2 \quad \text{if} \quad 2|\omega_0| > |\Omega| \\ |\omega_0| &< (u_{\max} - |\eta_0||\Omega|)/(1-|\eta_0|)^2 \quad \text{if} \quad 2|\omega_0| \le |\Omega| \end{aligned} \tag{91}$$

The control in Eq. (42) and the $\nu_{\max}$ given by Eq. (85) force uniform convergence of solutions to the model in Eq. (69) to the set of circular formations with radius $|\omega_0|^{-1}$ and the direction determined by the sign of ω_0.

Proof. Using the control in Eq. (42), observe that

$$\frac{\nu_k - \omega_0 s_k(t)}{K\omega_0 s_k(t)} = s_k(t)\langle e^{i\gamma_k}, P_k\boldsymbol{c}\rangle - \frac{\partial U}{\partial\psi_k}\frac{\omega_0 s_k(t)}{\omega_0 s_k(t) - \Omega} \tag{92}$$

Using the Lyapunov function in Eq. (39), substitute Eq. (92) into Eq. (41) to obtain

$$\dot V = \frac{1}{K\omega_0^2}\sum_{k=1}^{N}\frac{[\nu_k - \omega_0 s_k(t)]^2}{[s_k(t)]^2} \le 0 \quad \forall\ \nu_k \tag{93}$$

$\dot V$ is strictly less than zero, except when $-\nu_{\max} \le \nu_k \le \nu_{\max}$. In this interval, $\dot V \le 0$. This case is covered by Theorem 3. The rest of the proof follows from Lemma 7 and the proof of Theorem 3. □

VI. Coordinated Encirclement of a Maneuvering Target

In this section, consider the scenario of multiple unmanned vehicles following a maneuvering target so that the target forms the center of a circular formation. A nonrotating reference frame $\mathcal{B}$ is defined for which the origin O' is fixed to the target. O' moves with respect to the inertial frame $\mathcal{I}$ with a velocity and acceleration equal to the target velocity. Two path frames are used for particle k, as shown in Fig. 8. With no external flowfield, the kinematics in the inertial frame are given by the model in Eq. (3) with $f_k(t) = 0$. Integrating the following equations of motion (see Appendix B) yields r_k':

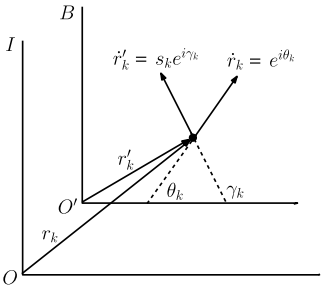

Fig. 8 Relationship between inertial frame $\mathcal{I}$ and accelerating frame $\mathcal{B}$ for particle k.

$$\dot r_k' = s_k(t)e^{i\gamma_k}; \qquad \dot\gamma_k = \nu_k \tag{94}$$

where $\dot s_k(t)$ is given by Eq. (B14). The inertial trajectory is

$$r_k(t) = r_k'(t) + \tfrac{1}{2}(a_x + ia_y)t^2 + [v_x(0) + iv_y(0)]t$$

The control laws developed in Sec. III with the model in Eq. (94) are used to assign the center point of the circular formation to a target in frame $\mathcal{B}$. The target-encirclement scenario is illustrated with three examples. In Sec. VI.A, a target is considered that is continuously accelerating and decelerating without turning. The magnitude of the velocity is always changing, but the direction is constant. Section VI.B illustrates the coordinated encirclement of a target that is traversing a circle of fixed radius and thus constantly changing its velocity direction while maintaining a fixed magnitude. For this flowfield, the time-phase parameter is used to regulate the temporal spacing of the particles. Section VI.C depicts the velocity of an actual target driving through an urban environment. This example shows the utility of the algorithms developed in Sec. IV to encircle a target in an estimated flowfield. Additionally, a turning rate constraint is imposed on the vehicles, as discussed in Sec. V. All of the examples illustrate realistic maneuvers of a mobile ground vehicle. In all the target-tracking examples, each autonomous vehicle measures the relative distance between it and the target.

A. Coordinated Encirclement of a Variable-Speed Target

This example replicates a target that is accelerating back and forth along a single trackline. Since the target velocity only varies in magnitude, it can be aligned with the real axis of an inertial frame without loss of generality. This scenario is illustrated using the control in Eq. (27) and the target acceleration

$$a_x(t) = \begin{cases} \frac{-4l}{T}, & \mathrm{mod}(t,T) < \frac{T}{2} \\ \frac{4l}{T}, & \mathrm{mod}(t,T) \ge \frac{T}{2} \end{cases} \tag{95}$$

where T and l represent the period and the maximum amplitude of the velocity, respectively. The target speed is greatest in the middle portion of the track and slows down and reverses direction at the edges.

Figure 9 illustrates the encirclement result of a target traversing with a period of $T = 150$ s and a maximum velocity equal to 75% of the particle's velocity ($l = 0.75$). Figure 9a shows the simulated results in an inertial reference frame. The target is aligned with the real axis and travels left and right without turning. In this figure, it is not apparent that the particles converge to a circular formation. However, this is readily seen in the target-centered frame, as illustrated with Figs. 9b and 9c. The target-centered figures illustrate the velocity by using the equivalent spatially uniform flowfield at that instance in time. Figure 9b shows the formation at $t = 400$ s; Fig. 9c

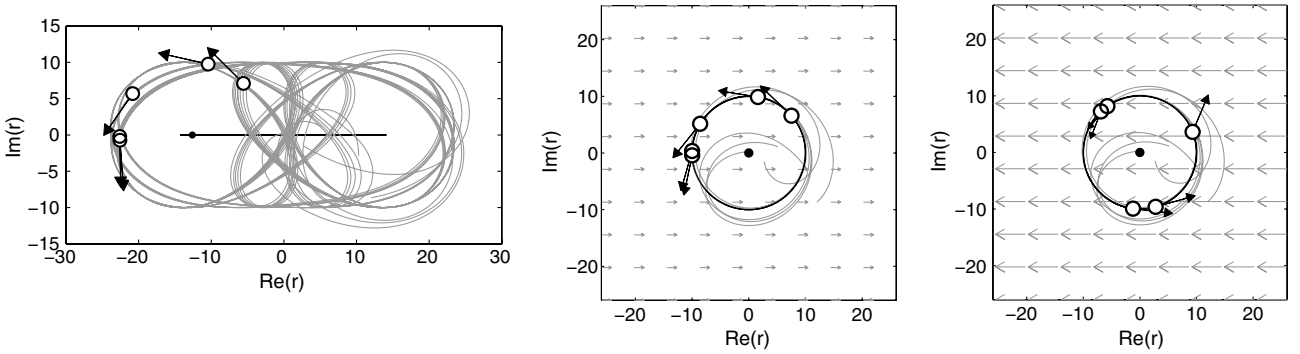

a) Inertial frame **b) Target frame, $t = 400$ *s*** **c) Target frame, $t = 600$ *s***

Fig. 9 Encirclement of a maneuvering target that is accelerating back and forth along a single trackline.

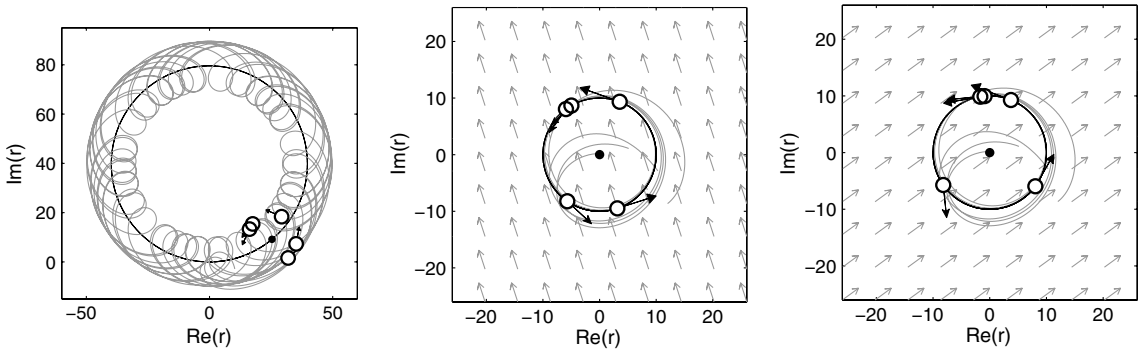

a) Inertial frame **b) Target frame, $t = 400$ *s*** **c) Target frame, $t = 800$ *s***

Fig. 10 Encirclement of a maneuvering target that is turning at a constant rate.

shows the formation at $t = 600$ s, when the target is traveling at its maximum velocity of $l = 0.75$.

B. Coordinated Encirclement of a Turning Target

This example illustrates the particle behavior as it follows a target performing a constant-rate turn of radius ρ. The target acceleration is $a_O(t) = (\eta_0^2/\rho) i e^{i2\pi t/T}$. The target has a fixed speed η_0 and a constantly changing direction of motion. Figure 10 illustrates the results of using the control algorithm in Eq. (27) with speed $\eta_0 = 0.5$ (50% of the particle's velocity) and the radius of curvature $\rho = 39.79$. The period of time it takes the target to traverse the circle is $T = 500$ s. Figure 10a illustrates the results in the inertial frame, showing the target track as it travels in a circle and the resulting particle tracks. Figures 10b and 10c display the simulation results in a target-fixed frame at $t = 400$ and 800 s, respectively. In these figures, the particles quickly converge to a circular formation and maintain that formation even as the target accelerates.

The turning-target scenario is also used to illustrate the control law in Eq. (42), which drives the particles to a time-splay formation. Figure 11 illustrates this example with $N = 5$ particles centered on a target circling at an angular rate of $\Omega = 2\pi/T$, a period of $T = 500$ s, and a target speed of $\eta_0 = 0.5$. Setting $\omega_0 = 0.1$ satisfies the requirement in Lemma 1. Figure 11a depicts the target and particles in the inertial frame. Figures 11b and 11c show the convergence to the time-splay configuration in the target-centered reference frame at $t = 800$ and 1000 s. These figures show that the particles converge to a time-splay formation even as the target accelerates.

C. Coordinated Encirclement of Maneuvering Target in an Urban Environment

In this example, the work of Secs. IV and V are combined to encircle a maneuvering target moving with an unknown velocity. The control algorithm in Eq. (60) was used to estimate the velocity of the target. Additionally, a turn-rate constraint is placed on the

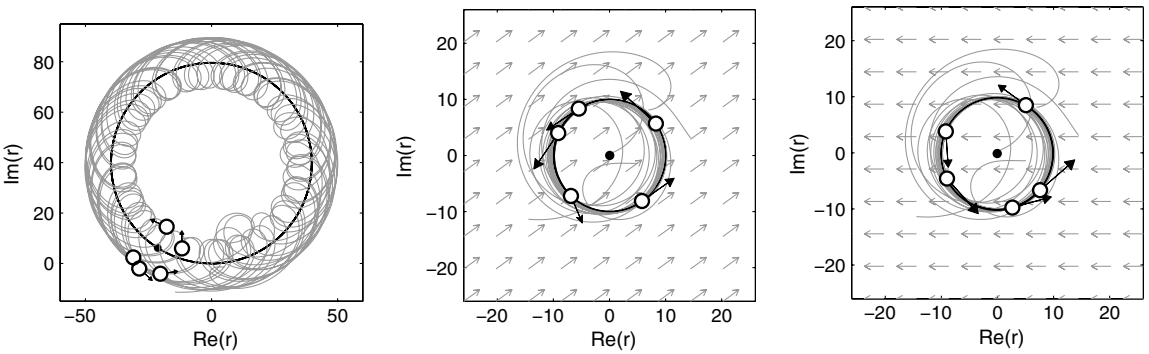

a) Inertial frame **b) Target frame, $t = 800$ *s*** **c) Target frame, $t = 1000$ *s***

Fig. 11 Coordinated encirclement of a maneuvering target that is turning at a constant rate.

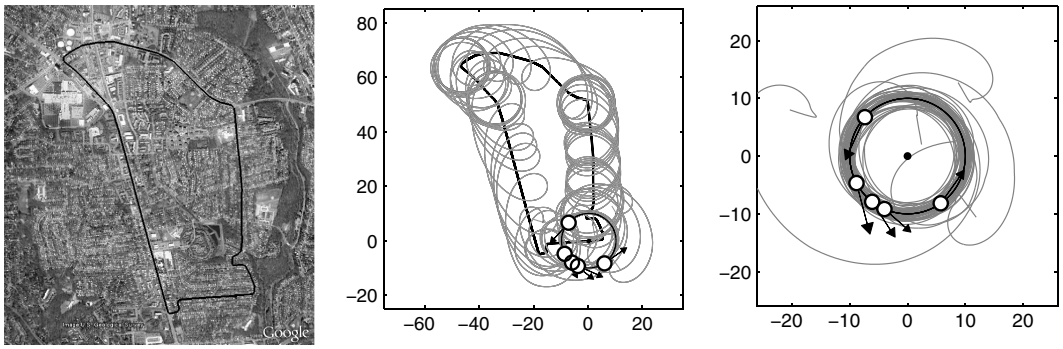

a) Target route **b) Inertial frame** **c) Target frame, $t = 1350\ s$**

Fig. 12 Coordinated encirclement of a target moving through urban traffic.

autonomous vehicles. The combined particle model for this simulation is

$$\dot{\hat{r}}_k = \hat{s}_k(t)e^{i\hat{\gamma}_k}; \qquad \dot{\hat{\gamma}}_k = \mathrm{sat}(\nu_k; \nu_{\max})$$

A set of Global Positioning System (GPS) waypoints is used to model the realistic behavior of a vehicle traveling in an urban environment. The vehicle tracks were collected during a 20 min. interval while driving through a Washington, D.C., suburb. The track included stops, turns, and other kinematic behavior typical in urban traffic. The maximum velocity of the target was 18.23 m/s (approximately 40 mph). It is assumed that the optimal velocity of the autonomous vehicles is 35 m/s. The velocity of the target and autonomous vehicles are normalized such that the autonomous vehicles travel at unit speed. (The normalized target velocity is 52% of the platform speed.) A turn rate of $u_{\max} = 0.23$ rad/s is imposed on the vehicles, which corresponds to a UAV maximum bank angle of 40° [4]. Following Eq. (75) from Lemma 6, a formation radius of $|\omega_0|^{-1} = 10$ was chosen.

Figure 12 shows the results from the urban-traffic scenario. Figure 12a displays the GPS waypoints on a street map of the area. The movement of the target-fixed frame was generated from these waypoints by converting the GPS latitude and longitude points into a topocentric North-East-Down coordinate frame centered on the starting location. In this frame, the distances between the waypoints and their associated timestamps were used to determine the velocity of the target vehicle. The target velocity is piecewise constant, because it is constructed out of a discrete set of waypoints and does not consider acceleration. Discontinuities of the velocity are especially pronounced when the vehicle turns sharply, as both the direction and magnitude may change suddenly. Although the velocity of the target is being estimated, the vehicle is able to measure the relative position between itself and the target. Figure 12b displays both the target and vehicle tracks in the inertial frame. (The distance units are based upon the normalized speed of the ground vehicle.) The figure shows separations in the vehicle tracks that correspond to the velocity of the target. When the target is traveling quickly, the cyclic tracks are spaced further apart than in the slower-moving parts of the track. The points at which the target is stopped (due to traffic lights) are evident by the track circle over that point. Figure 12c shows the circular formation in the target-fixed frame for the 20 min. time interval. This figure highlights the effect of the velocity discontinuities on the formation: particles exhibit a period of transient behavior after each maneuver before converging to a circular formation.

VII. Conclusions

Cooperative control improves the capacity of unmanned vehicles to gather information, track targets, and perform autonomous missions. The decentralized control algorithms presented in this paper regulate vehicle formations in a spatiotemporal flowfield of moderate strength. For a known spatially or temporally varying flowfield, a time-splay configuration can also be generated. If the flowfield is unknown, an estimated flowfield is used to stabilize circular formations in a spatially invariant flowfield. Additionally, dynamic circular and time-splay algorithms are derived for estimated time-varying flowfields. These algorithms are shown to be robust to bounds on the turn rate of the vehicle. These algorithms provide the capability to cooperatively encircle maneuvering targets that turn, accelerate, and operate in an urban environment, as was illustrated in the simulations. Ongoing work seeks to expand the class of flowfields in which the results apply, such as flowfields that exceed the particle speed relative to the flow.

Appendix A: Estimation-Error Eigenvalues for a Rotating Flowfield

In this Appendix, the real portion of the eigenvalues of matrix B, defined in Eq. (62), is derived:

$$\lambda = \frac{-(K_1 - \Omega i) \pm \sqrt{(K_1 - \Omega i)^2 - 4(-K_1\Omega i + K_2)}}{2}$$
$$= \frac{-K_1 + \Omega i \pm \sqrt{(K_1^2 - \Omega^2 - 4K_2) + (2K_1\Omega)i}}{2}$$

The real parts of the eigenvalues are

$$Re(\lambda) = \frac{-K_1 \pm Re[\sqrt{(K_1^2 - \Omega^2 - 4K_2) + (2K_1\Omega)i}]}{2} \tag{A1}$$

To find the real part of the square-root term, which contains a complex number, observe that

$$Re(\sqrt{a + bi}) = Re(\sqrt{\rho e^{\phi i}}) = \sqrt{\rho}\cos\frac{\phi}{2}$$

with $\rho = \sqrt{a^2 + b^2}$ and $\cos\phi = a/\rho$. Using the half-angle formula for $\cos\phi = \sqrt{(1 + \cos 2\phi)/2}$, the real part of the square root becomes

$$Re(\sqrt{a + bi}) = \sqrt{\rho}\sqrt{\left(\frac{1 + a/\rho}{2}\right)} = \sqrt{\frac{\rho + a}{2}}$$

Substituting into Eq. (A1) yields

$$Re(\lambda) = \frac{-K_1}{2} \pm \frac{\sqrt{\sqrt{(K_1^2 - \Omega^2 - 4K_2)^2 + 4K_1^2\Omega^2} + (K_1^2 - \Omega^2 - 4K_2)}}{2\sqrt{2}}$$

which is the real portion of the eigenvalues of matrix B.

Appendix B: Particle Speed in an Accelerating Frame

In this Appendix, we develop the inertial speed $s_k(t)$ for a Newtonian particle traveling in an accelerating frame. With no external flowfield, the kinematics in the inertial frame are

$$\dot{r}_k = e^{i\theta_k} \tag{B1}$$

$$\ddot{r}_k = \dot{\theta}_k i e^{i\theta_k} \tag{B2}$$

The steering control is $\dot{\theta}_k = u_k$. Let r'_k be the position of the particle k relative to O'. The inertial kinematics relative to O' are

$$\dot{r}'_k \triangleq s_k(t) e^{i\gamma_k} \tag{B3}$$

$$\ddot{r}'_k = \dot{s}_k(t) e^{i\gamma_k} + s_k(t)\dot{\gamma}_k i e^{i\gamma_k} \tag{B4}$$

The magnitude and orientation of $\dot{r}'_k$ are $s_k(t)$ and γ_k. Let $r_{O'}$ be the position of O' with respect to O. By vector addition, we have

$$\ddot{r}'_k = \ddot{r}_k - \ddot{r}_{O'} \tag{B5}$$

The velocity and acceleration between frames $\mathcal{I}$ and $\mathcal{B}$ are defined to be $\dot{r}'_O = v_O = v_x + iv_y$ and $\ddot{r}'_O = a_O = a_x + ia_y$, respectively. To find the equations of motion for the particle k in frame $\mathcal{B}$, substitute Eqs. (B2) and (B4) into Eq. (B5), which yields

$$\dot{s}_k(t) e^{i\gamma_k} + s_k(t)\dot{\gamma}_k i e^{i\gamma_k} = u_k i e^{i\theta_k} - a_x - ia_y \tag{B6}$$

From Fig. 8 and Euler's formula, observe that

$$i e^{i\theta_k} = \sin(\gamma_k - \theta_k) e^{i\gamma_k} + \cos(\gamma_k - \theta_k) i e^{i\gamma_k} \tag{B7}$$

$$a_x = a_x(\cos\gamma_k e^{i\gamma_k} - \sin\gamma_k i e^{i\gamma_k}) \tag{B8}$$

$$a_y = a_y(\sin\gamma_k e^{i\gamma_k} + \cos\gamma_k i e^{i\gamma_k}) \tag{B9}$$

Substituting Eqs. (B7–B9) into Eq. (B6) yields

$$\dot{s}_k(t) = u_k \sin(\gamma_k - \theta_k) - a_x \cos\gamma_k - a_y \sin\gamma_k \tag{B10}$$

$$\dot{\gamma}_k = \frac{1}{s_k(t)}[u_k \cos(\gamma_k - \theta_k) + a_x \sin\gamma_k - a_y \cos\gamma_k] \triangleq \nu_k \tag{B11}$$

Solving Eq. (B11) for u_k and substituting into Eq. (B10) gives

$$\dot{s}_k(t) = [s_k(t)\nu_k - a_x \sin\gamma_k + a_y \cos\gamma_k]\tan(\gamma_k - \theta_k) - a_x \cos\gamma_k - a_y \sin\gamma_k \tag{B12}$$

To eliminate θ_k from Eq. (B12), use

$$s_k(t) e^{i\gamma_k} = e^{i\theta_k} - v_O; \qquad s_k(t) e^{i(\gamma_k - \theta_k)} = 1 - v_O e^{-i\theta_k}$$

Equating the real and imaginary parts of the previous equations yields

$$s_k(t)\cos\gamma_k = \cos\theta_k - v_x; \qquad s_k(t)\sin\gamma_k = \sin\theta_k - v_y$$

and

$$\begin{aligned} s_k(t)\cos(\gamma_k - \theta_k) &= 1 - v_x\cos\theta_k - v_y\sin\theta_k \\ &= 1 - v_x(v_x + s_k(t)\cos\gamma_k) - v_y(v_y + s_k(t)\sin\gamma_k) \\ s_k(t)\sin(\gamma_k - \theta_k) &= v_x\sin\theta_k - v_y\cos\theta_k = v_x s_k(t)\sin\gamma_k \\ &\quad - v_y s_k(t)\cos\gamma_k \\ \tan(\gamma_k - \theta_k) &= \frac{v_x s_k(t)\sin\gamma_k - v_y s_k(t)\cos\gamma_k}{[1 - v_x^2 - v_y^2 - v_x s_k(t)\cos\gamma_k - v_y s_k(t)\sin\gamma_k]} \end{aligned} \tag{B13}$$

Substituting Eq. (B13) into Eq. (B12) yields

$$\begin{aligned} \dot{s}_k(t) &= \frac{[s_k(t)\nu_k - a_x\sin\gamma_k + a_y\cos\gamma_k][v_x s_k(t)\sin\gamma_k - v_y s_k(t)\cos\gamma_k]}{1 - v_x^2 - v_y^2 - v_x s_k(t)\cos\gamma_k - v_y s_k(t)\sin\gamma_k} \\ &\quad - a_x\cos\gamma_k - a_y\sin\gamma_k \end{aligned} \tag{B14}$$

Acknowledgments

This material is based upon work supported by the National Science Foundation, under grant number CMMI0928416, and the Office of Naval Research, grant number N00014-09-1-1058.

References

[1] Elston, J., and Frew, E., "Unmanned Aircraft Guidance for Penetration of Pre-Tornadic Storms," *Journal of Guidance, Control, and Dynamics*, Vol. 33, No. 1, 2010, pp. 99–107. doi:10.2514/1.45195

[2] Frew, E. W., Lawrence, D. A., and Morris, S., "Coordinated Standoff Tracking of Moving Targets Using Lyapunov Guidance Vector Fields," *Journal of Guidance, Control, and Dynamics*, Vol. 31, No. 2, 2008, pp. 290–306. doi:10.2514/1.30507

[3] Summers, T. H., Akella, M. R., and Mears, M. J., "Coordinated Standoff Tracking of Moving Targets: Control Laws and Information Architectures," *Journal of Guidance, Control, and Dynamics*, Vol. 32, No. 1, 2009, pp. 56–69. doi:10.2514/1.37212

[4] Wise, R., and Rysdyk, R., "UAV Coordination for Autonomous Target Tracking," AIAA Guidance, Navigation, and Control Conference, Keystone, CO, AIAA Paper 2006-6453, Aug. 2006.

[5] Justh, E. W., and Krishnaprasad, P. S., "Equilibria and Steering Laws for Planar Formations," *Systems and Control Letters*, Vol. 52, No. 1, 2004, pp. 25–38. doi:10.1016/j.sysconle.2003.10.004

[6] Sepulchre, R., Paley, D. A., and Leonard, N. E., "Stabilization of Planar Collective Motion: All-to-All Communication," *IEEE Transactions on Automatic Control*, Vol. 52, No. 5, 2007, pp. 811–824. doi:10.1109/TAC.2007.898077

[7] Sepulchre, R., Paley, D. A., and Leonard, N. E., "Stabilization of Planar Collective Motion with Limited Communication," *IEEE Transactions on Automatic Control*, Vol. 53, No. 3, 2008, pp. 706–719. doi:10.1109/TAC.2008.919857

[8] Olfati-Saber, R., and Murray, R., "Graph Rigidity and Distributed Formation Stabilization of Multi-Vehicle Systems," *IEEE Conference on Decision and Control*, Vol. 3, IEEE Publ., Piscataway, NJ, 2002, pp. 2965–2971.

[9] Kingston, D. B., "Decentralized Control of Multiple UAVs for Perimeter and Target Surveillance," Ph.D. Thesis, Department of Electrical and Computer Engineering, Brigham Young Univ., Provo, UT, Dec. 2007.

[10] Fax, J. A., and Murray, R. M., "Information Flow and Cooperative Control of Vehicle Formations," *IEEE Transactions on Automatic Control*, Vol. 49, No. 9, 2004, pp. 1465–1476. doi:10.1109/TAC.2004.834433

[11] Techy, L., Woolsey, C. A., and Schmale, D. G., "Path Planning for Ecient UAV Coordination in Aerobiological Sampling Missions," *Proceedings of the IEEE Conference on Decision and Control*, Cancun, Mexico, IEEE Publ., Piscataway, NJ, Dec. 2008, pp. 2814–2819.

[12] Fiorelli, E., Leonard, N., Bhatta, P., Paley, D., Bachmayer, R., and Fratantoni, D., "Multi-AUV Control and Adaptive Sampling in Monterey Bay," *IEEE Journal of Oceanic Engineering*, Vol. 31, No. 4, 2006, p. 935. doi:10.1109/JOE.2006.880429

[13] Hsieh, C., Jin, Z., Marthaler, D., Nguyen, B., Tung, D., Bertozzi, A., and Murray, R., "Experimental Validation of an Algorithm for Cooperative Boundary Tracking," *Proceedings of the 2005 American Control Conference*, Vol. 2, IEEE Publ., Piscataway, NJ, 2005, pp. 1078–1083.

[14] Klein, D. J., and Morgansen, K. A., "Controlled Collective Motion for Trajectory Tracking," *Proceedings of the 2006 American Control Conference*, Minneapolis, MN, IEEE Publ., Piscataway, NJ, June 2006, pp. 5269–5275.

[15] Ceccarelli, N., Enright, J. J., Frazzoli, E., Rasmussen, S. J., and Schumacher, C. J., "Micro UAV Path Planning for Reconnaissance in Wind," *Proceedings of the 2007 American Control Conference*, New York, IEEE Publ., Piscataway, NJ, July 2007, pp. 5310–5315.

[16] McGee, T. G., Spry, S., and Hedrick, J. K., "Optimal Path Planning in a Constant Wind with a Bounded Turning Rate," *AIAA Conference on Guidance, Navigation, and Control*, San Francisco, CA, AIAA Paper 2005-6186, Aug. 2005.

[17] Paley, D. A., "Stabilization of Collective Motion in a Uniform and Constant Flow Field," *AIAA Guidance, Navigation, and Control Conference and Exhibit*, Honolulu, HI, AIAA Paper 2008-7173, Aug. 2008.

[18] Paley, D. A., and Peterson, C., "Stabilization of Collective Motion in a Time-Invariant Flowfield," *Journal of Guidance, Control, and Dynamics*, Vol. 32, No. 3, 2009, pp. 771–779. doi:10.2514/1.40636

[19] Paley, D. A., Techy, L., and Woolsey, C. A., "Coordinated Perimeter Patrol with Minimum-Time Alert Response," *AIAA Guidance, Navigation, and Control Conference*, AIAA Paper 2009-6210, Aug. 2009.

[20] Techy, L., Paley, D. A., and Woolsey, C. A., "Unmanned Aerial Vehicle Coordination on Closed Convex Paths in Wind," *Journal of Guidance, Control, and Dynamics*, Vol. 33, No. 6, 2010, pp. 1946–1951. doi:10.2514/1.47655

[21] Grocholsky, B., Durrant-Whyte, H., and Gibbens, P., "An Information-Theoretic Approach to Decentralized Control of Multiple Autonomous Flight Vehicles," *Sensor Fusion and Decentralized Control in Robotic Systems Conference*, Vol. 4196, Society of Photo-Optical Instrumentation Engineers, Bellingham, WA, 2000, pp. 348–359.

[22] Ousingsawat, J., and Campbell, M., "Establishing Trajectories for Multi-Vehicle Reconnaissance," AIAA Guidance, Navigation, and Control Conference, Providence, RI, AIAA Paper 2004-5224, Aug. 2004.

[23] Zhou, K., and Roumeliotis, S., "Optimal Motion Strategies for Range-Only Constrained Multisensor Target Tracking," *IEEE Transactions on Robotics and Automation*, Vol. 24, No. 5, 2008, pp. 1168–1185. doi:10.1109/TRO.2008.2004488

[24] Fax, J. A., and Murray, R. M., "Graph Laplacians and Stabilization of Vehicle Formations," *Proceedings of the 15th IFAC World Congress*, Barcelona, International Federation of Automatic Control, Laxenburg, Austria, July 2002, pp. 283–288.

[25] Khalil, H. K., "Advanced Stability Analysis," *Nonlinear Systems*, 3rd ed., Prentice–Hall, Upper Saddle River, NJ, 2002, pp. 303–338, Chap. 8.

[26] Richards, A., and How, J., "Aircraft Trajectory Planning with Collision Avoidance Using Mixed Integer Linear Programming," *Proceedings of the American Control Conference*, Vol. 3, IEEE Publ., Piscataway, NJ, 2002, pp. 1936–1941.